

NIST Technical Note 1877

Quantitative Imaging of Clinker and Cement Microstructure

Paul E. Stutzman
Jeffrey W. Bullard
Pan Feng

This publication is available free of charge from:
<http://dx.doi.org/10.6028/NIST.TN.1877>

NIST Technical Note 1877

Quantitative Imaging of Clinker and Cement Microstructure

Paul E. Stutzman¹
Jeffrey W. Bullard¹
Pan Feng^{1,2}

¹*Materials and Structural Systems Division
Engineering Laboratory*

²*Southeast University, Nanjing, Jiangsu 210096, China*

This publication is available free of charge from:
<http://dx.doi.org/10.6028/NIST.TN.1877>

April 2015



U.S. Department of Commerce
Penny Pritzker, Secretary

National Institute of Standards and Technology
Willie May, Acting Under Secretary of Commerce for Standards and Technology and Acting Director

Certain commercial entities, equipment, or materials may be identified in this document in order to describe an experimental procedure or concept adequately. Such identification is not intended to imply recommendation or endorsement by the National Institute of Standards and Technology, nor is it intended to imply that the entities, materials, or equipment are necessarily the best available for the purpose.

National Institute of Standards and Technology Technical Note 1877
Natl. Inst. Stand. Technol. Tech. Note 1877, 46 pages (April 2015)
CODEN: NTNOEF

This publication is available free of charge from:
<http://dx.doi.org/10.6028/NIST.TN.1877>

Abstract

The combination of scanning electron microscopy (SEM) with X-ray microanalysis and image processing provides a powerful ability to image and quantify microstructural features of construction materials. This document provides guidance for collecting backscattered electron images and X-ray element maps of polished sections of Portland cement clinker. It furnishes step-by-step procedures for processing image data to produce segmentation of an image field into its constituent mineral phases, and describes ways use the segmented image to measure the abundance, surface area, and spatial distribution of phases in the image field. Inherent heterogeneity of the microstructure implies that different image fields of the same material will contain different phase abundances; the document suggests ways to estimate and compensate for the heterogeneity length scale through statistical analysis of multiple image fields. and analysis using a scanning electron microscope will be illustrated using an example from the development of Standard Reference Materials for portland cement clinker.

Contents

List of Tables iii

List of Figures iv

1 Introduction 1

2 Specimen Preparation 2

2.1 Carbon Coating for Imaging 3

2.2 Sample Storage 4

2.3 SEM Imaging 4

2.4 X-Ray Microanalysis and Imaging 5

3 Application to SRM 2686a 6

3.1 Image Processing 10

3.2 Visualizing Phase Occurrence and Distribution by Color Merge 14

3.3 Image Processing with MultiSpec 14

3.4 Cleaning up the segmented image 21

3.5 Quantitative Image Analysis 23

3.5.1 Installing MicroChar 24

3.5.2 Using MicroChar 24

3.5.3 Two-point correlation functions 27

3.6 Larger Image Field 30

3.7 Multiple Image Statistics for SRM 2686a 32

Appendix A Step-by Step Summary for Clinker Analysis 34

References 38

List of Tables

1	Clinker phases, compositions, densities, average atomic number, and backscattered electron coefficient ranked according to relative SEM BE image brightness [17].	5
2	Textural and chemical characteristics useful for distinguishing clinker phases. . .	6
3	Comparison of clinker phase mass fractions, expressed as a percentage of total solids, estimated for SRM 2686a from the larger field of view in Fig. 30 to the certified values [15]. Measurements are based on one image field, so no uncertainty estimate is given.	31
4	SRM 2686a phase fractions expressed as a mass percent by field and a running average.	33

List of Figures

1	An early thin section micrograph (1917) of belite crystals bounded by dark gray tricalcium aluminate domains (90×, crossed Nichols [2]).	2
2	Clinker microscopists relate textural characteristics to raw mix proportioning, homogenization, and clinkering processes, as from Hoffmännner [9].	3
3	Energy-dispersive X-ray microanalysis shows spectra from the primary clinker phases exhibit characteristic spectra on a continuous background and standard-based quantitative analysis of chemical composition expressed as oxides.	7
4	SEM backscattered electron image of SRM 2686a, showing a medium-grained, heterogeneous silicate distribution and a coarse-grained matrix with phase identifications. Field width is 256 μm.	8
5	X-ray microanalysis images of the spatial distribution of elements for the field of view shown in Figure 4. The image in the upper left is the BE image. Field width is 256 μm.	9
6	Reducing noise associated with the continuous spectrum background improves the delineation of aphtitalite from the raw Na XR image (left) and histogram, as shown in the processed subtracted image (right). Field width is 256 μm.	10
7	Mg XR map associated with low concentrations in the silicates and matrix phases may confound segmentations. Subtracting low-level signal associated with background and low concentrations of Mg presents a clearer rendering of periclase location. Field width is 256 μm.	11
8	Thresholded blur filter applied to the BE image removes minor scratch marks and makes the gray levels for each phase more uniform as seen in the images and gray level histograms. Field width is 256 μm.	12
9	Thresholded Blur algorithm applied to the Ca X-ray image improves the distinction between phases by comparing gray level histograms from the initial (A) and filtered (B) images, which now shows distinct peaks for alite, belite and matrix. Field width is 256 μm.	13
10	Composite image with the BE as red, Mg as green, Al as blue and S as yellow illustrates how the addition of the X-ray data improves phase identification. Alite is a brighter red than belite, the matrix phases are bluish (aluminate) and pink (ferrite), periclase is green, and alkali sulfates are yellow. Field width is 256 μm.	13
11	Loading the SEM BE image in MultiSpec interprets the image file details with an enhancement option to trim a percentage of the high- and low-end signal, if necessary.	16
12	Linking the BE image to a set of XR images from the same field of view is accomplished in MultiSpec by selecting each XR image, specifying “Link selected file(S) to active image window” in the drop-down menu, and completed by selecting <i>Cancel</i>	17

13	Saving the linked BE and X-ray images using the <i>Processor</i> → <i>Reformat</i> → <i>Rectify</i> provides a chance to subsample the set and repair any image registration issues (rectification).	17
14	Selecting the linked, rectified multispectral image set, indicated by file extension .LAN will allow display of the image set and establishing training fields.	18
15	Three-color (RGB) display by channel will provide a rendering of phase distribution for the next step of establishing the training fields.	18
16	MultiSpec <i>Image</i> → <i>Display</i> allows three channels to be assigned to Red-Green-Blue color planes to facilitate identification of phase type and distribution. The upper image is BE (red), Mg (green), and Al (blue) while the lower is BE (red), K (green), and Na (blue). Field width is 256 μm	19
17	Training fields are defined by boxing regions typical for each phase (class) and assigning a class name. Additional training fields are created by selecting a phase, boxing a new region, and adding it to the class.	19
18	Classification is initiated by selection of a procedure, the use or exclusion of some image channels, and writing the classification results to a disk file.	20
19	MultiSpec classification table, or accuracy matrix, shows the classification set assignment accuracy, incorrectly assigned pixel counts, an overall accuracy assessment by the Kappa statistic, and the area fraction for each class [12]. Data shown here are based on one image, so no uncertainty statement is possible. The “Reliability Accuracy” value for each phase refers to the percentage of training set pixels that are correctly reclassified by the segmentation as the phase to which they were originally assigned.	22
20	Comparing the segmented image to the original BE image (Fig. 4) indicates a successful segmentation. Some incorrectly assigned pixels occur at grain boundaries and within belite, which will be repaired in the final processing step. Field width is 256 μm	22
21	Original SEM BE image (left) and the processed, segmented indexed image (right) for comparison. Segmentation used the Fisher Linear Likelihood algorithm. Field width is 256 μm	23
22	Installation of MicroChar on Mac OS X computers.	24
23	MicroChar main window.	25
24	Phase identification is accomplished in MicroChar by accepting the default settings or by selecting the phases from the series of pull down menus.	26
25	Files produced by MicroChar store the results of its calculations.	26
26	Contents of the pfc file for the segmented image of SRM 2686a in Fig. 20. Here the column heading “Volume” corresponds to the phase area fractions and “Area” to the perimeter fraction.	27
27	(a) False color PNG image of SRM 2686 microstructure, and (b) the phase boundaries. Field width is 256 μm	27

28	(a) Contents of the alite two-point correlation function data file for SRM 2686a image in Fig. 20 with distance in the first column and probability density in the second column; (b) plot of the two-point correlation function S_2 for alite and for belite in the SRM 2686a image (right).	28
29	Two-point correlation functions for periclase and arcanite in SRM 2686a. Note the two different scales on the y -axes.	29
30	Larger image field of SRM 2686a. Magnification 300 \times , 1024 \times 768 pixels. (a) False color PNG image, and (b) the phase mass, volume, and area fractions. Field width is 1.536 mm.	30
31	Two-point correlation functions calculated for alite and belite using the large image field of SRM 2686a shown in Fig. 30.	31
32	Running average plots for SEM/IA analysis of SRM2686a shows values beginning to stabilize after about five image fields.	34
33	Box plots by phase for SEM analysis of SRM 2686a. Stars indicate certified values.	35

1 Introduction

Microstructural analysis of cementitious materials by microscopy dates back over 100 years when Henri Le Châtelier [13] investigated portland cement clinker using what was, at the time, a new polarized light microscopy method. He documented the optical properties of the main phases and identified tricalcium silicate as the principal constituent of portland cement clinker. Subsequent work by A.E. Tornebohm, Bates and Klein [2] (see Fig. 1), and others provided a more detailed description of the phases and textures of clinker and also developed the techniques for light microscopy as it applies to portland cement clinker [11]. More recent resources for clinker microscopy include the work of Campbell [6] and of Hofmänner [9]. Quantitative microscopy methods began with Delesse [7], who recognized the relationship between the area fraction of a mineral in a 2D section and its 3D volume fraction in the material. The first quantitative procedures involved sketching on paper the observed microstructure, tracing the grain outlines onto a metal foil, and finally cutting and weighing the mineral constituents from the foil traces. These quantitative methods evolved by subsampling the microstructure through linear traverse and point sampling to achieve quantitative estimates of mineral abundance. These latter methodologies, although more than a century old and quite time consuming, are still used today in many disciplines for quantitative phase analysis.

The combination of the scanning electron microscope (SEM) with image analysis has in some ways brought quantitative microscopy back to its roots. Traditional point count and linear traverse methods may still be applied to images generated by the SEM, but the SEM can be further exploited to produce a set of high-resolution image fields from a single material. These image sets are sufficiently uniform that feature extraction and quantitative measurement by digital image processing are possible. In this case, the mineral constituents are digitally traced and extracted from the bulk microstructure by a set of operations termed *image processing* and *image analysis*, which supplant the older weighing operations with semi-automated pixel counting to determine phase abundance. The potential for automation in the data collection and processing promises to provide for a much greater sampling of any microstructure and quantitative estimates of microstructural features that were not easily accomplished in the past.

This report describes imaging and analysis procedures for portland cement clinker using SEM with backscattered electron (BE), X-ray microanalysis (XR), image processing and image analysis. The procedures are used to uniquely identify and separate a microstructure image into its constituent phases, a process known as segmentation. Segmented images can be used to make quantitative measurements such as phase abundance and surface area fractions.

It should be stated clearly at the outset that, for several reasons, microstructure imaging and image analysis have always had—and likely will continue to have—a partially subjective aspect. First, microstructure is not a well-defined material property. It is often characterized by significant chemical and spatial heterogeneity that can be measured only in a statistical sense, and the principles of uncertainty estimates for image analysis are largely undeveloped. Second, both an electron beam's interaction with the specimen and the digitized nature of a microstructure image causes a level of coarse graining in which volume is homogenized into small elements that cannot be resolved more finely than a single pixel. But neither chemical nor phase composition of the ac-

tual microstructure is constrained to the pixel scale; solid solutions and finely divided phases can cause variations in contrast that, when averaged over the pixel volume, can make phase assignments uncertain for some pixels, especially at interphase boundaries and within the interstitial phase regions. The fraction of such “borderline” pixels is usually small within any image, but no single objective method is currently available for infallibly assigning their phase identity. Instead, for these cases the user must appeal to several types of possibly inconsistent data about a pixel or pixel grouping, such as its backscattered contrast, X-ray element signal, and location within the microstructure, and arrive at an informed judgment based on experience. Therefore, phrases used in this report, such as “accurate phase assignment,” or “incorrectly assigned pixels” should be qualified in terms of the best judgment of an experienced user.

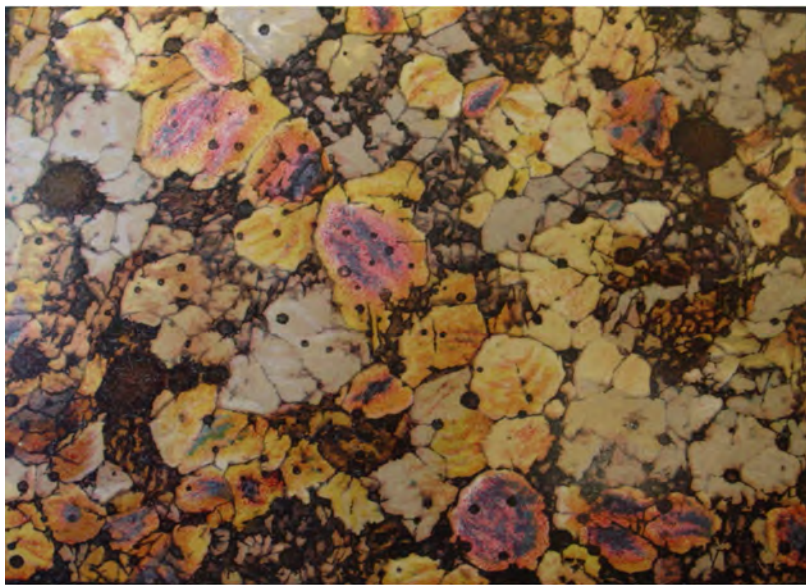


Figure 1: An early thin section micrograph (1917) of belite crystals bounded by dark gray tricalcium aluminate domains (90 \times , crossed Nichols [2]).

2 Specimen Preparation

The sample taken for analysis should be as representative of the bulk material as possible. However, aside from ASTM C183 [1], no guide or standardized procedure is available for clinker or cements. Sample splitters or the cone-and-quarter method may be used to reduce large-volume samples to representative subsamples, and down to a volume suitable for making an epoxy-embedded specimen mount. A medium-viscosity epoxy¹² is suitable for the mount because it

¹Epotek 301, Epoxy Technology, Inc., 14 Fortune Drive, Billerica, MA 01821

²Certain commercial entities, equipment, or materials are identified in this document in order to describe an experimental procedure or concept adequately. Such identification is not intended to imply recommendation or endorsement by the National Institute of Standards and Technology, nor is it intended to imply that the entities,

FREE LIME										Characteristic fabric features	
None		Homogeneously distributed		Diffuse clusters		Relict clusters		Superficial clusters			
Belite		Belite		Belite		Belite		Belite			
Little to none		Little to none		Little to none		Little to none		Little to none		Little to none	
Diffuse clusters		Diffuse clusters		Diffuse clusters		Diffuse clusters		Diffuse clusters		Diffuse clusters	
Streaks		Streaks		Streaks		Streaks		Streaks		Streaks	
Homogeneously distributed		Homogeneously distributed		Homogeneously distributed		Homogeneously distributed		Homogeneously distributed		Homogeneously distributed	
Little to none		Little to none		Little to none		Little to none		Little to none		Little to none	
Diffuse clusters		Diffuse clusters		Diffuse clusters		Diffuse clusters		Diffuse clusters		Diffuse clusters	
Streaks		Streaks		Streaks		Streaks		Streaks		Streaks	
Homogeneously distributed		Homogeneously distributed		Homogeneously distributed		Homogeneously distributed		Homogeneously distributed		Homogeneously distributed	
Little to none		Little to none		Little to none		Little to none		Little to none		Little to none	
Diffuse clusters		Diffuse clusters		Diffuse clusters		Diffuse clusters		Diffuse clusters		Diffuse clusters	
Streaks		Streaks		Streaks		Streaks		Streaks		Streaks	
Homogeneously distributed		Homogeneously distributed		Homogeneously distributed		Homogeneously distributed		Homogeneously distributed		Homogeneously distributed	
Little to none		Little to none		Little to none		Little to none		Little to none		Little to none	
Diffuse clusters		Diffuse clusters		Diffuse clusters		Diffuse clusters		Diffuse clusters		Diffuse clusters	
Streaks		Streaks		Streaks		Streaks		Streaks		Streaks	
Homogeneously distributed		Homogeneously distributed		Homogeneously distributed		Homogeneously distributed		Homogeneously distributed		Homogeneously distributed	
Little to none		Little to none		Little to none		Little to none		Little to none		Little to none	
Diffuse clusters		Diffuse clusters		Diffuse clusters		Diffuse clusters		Diffuse clusters		Diffuse clusters	
Streaks		Streaks		Streaks		Streaks		Streaks		Streaks	
Homogeneously distributed		Homogeneously distributed		Homogeneously distributed		Homogeneously distributed		Homogeneously distributed		Homogeneously distributed	
Little to none		Little to none		Little to none		Little to none		Little to none		Little to none	
Diffuse clusters		Diffuse clusters		Diffuse clusters		Diffuse clusters		Diffuse clusters		Diffuse clusters	
Streaks		Streaks		Streaks		Streaks		Streaks		Streaks	
Homogeneously distributed		Homogeneously distributed		Homogeneously distributed		Homogeneously distributed		Homogeneously distributed		Homogeneously distributed	
Little to none		Little to none		Little to none		Little to none		Little to none		Little to none	
Diffuse clusters		Diffuse clusters		Diffuse clusters		Diffuse clusters		Diffuse clusters		Diffuse clusters	
Streaks		Streaks		Streaks		Streaks		Streaks		Streaks	
Homogeneously distributed		Homogeneously distributed		Homogeneously distributed		Homogeneously distributed		Homogeneously distributed		Homogeneously distributed	
Little to none		Little to none		Little to none		Little to none		Little to none		Little to none	
Diffuse clusters		Diffuse clusters		Diffuse clusters		Diffuse clusters		Diffuse clusters		Diffuse clusters	
Streaks		Streaks		Streaks		Streaks		Streaks		Streaks	
Homogeneously distributed		Homogeneously distributed		Homogeneously distributed		Homogeneously distributed		Homogeneously distributed		Homogeneously distributed	
Little to none		Little to none		Little to none		Little to none		Little to none		Little to none	
Diffuse clusters		Diffuse clusters		Diffuse clusters		Diffuse clusters		Diffuse clusters		Diffuse clusters	
Streaks		Streaks		Streaks		Streaks		Streaks		Streaks	
Homogeneously distributed		Homogeneously distributed		Homogeneously distributed		Homogeneously distributed		Homogeneously distributed		Homogeneously distributed	
Little to none		Little to none		Little to none		Little to none		Little to none		Little to none	
Diffuse clusters		Diffuse clusters		Diffuse clusters		Diffuse clusters		Diffuse clusters		Diffuse clusters	
Streaks		Streaks		Streaks		Streaks		Streaks		Streaks	
Homogeneously distributed		Homogeneously distributed		Homogeneously distributed		Homogeneously distributed		Homogeneously distributed		Homogeneously distributed	
Little to none		Little to none		Little to none		Little to none		Little to none		Little to none	
Diffuse clusters		Diffuse clusters		Diffuse clusters		Diffuse clusters		Diffuse clusters		Diffuse clusters	
Streaks		Streaks		Streaks		Streaks		Streaks		Streaks	
Homogeneously distributed		Homogeneously distributed		Homogeneously distributed		Homogeneously distributed		Homogeneously distributed		Homogeneously distributed	
Little to none		Little to none		Little to none		Little to none		Little to none		Little to none	
Diffuse clusters		Diffuse clusters		Diffuse clusters		Diffuse clusters		Diffuse clusters		Diffuse clusters	
Streaks		Streaks		Streaks		Streaks		Streaks		Streaks	
Homogeneously distributed		Homogeneously distributed		Homogeneously distributed		Homogeneously distributed		Homogeneously distributed		Homogeneously distributed	
Little to none		Little to none		Little to none		Little to none		Little to none		Little to none	
Diffuse clusters		Diffuse clusters		Diffuse clusters		Diffuse clusters		Diffuse clusters		Diffuse clusters	
Streaks		Streaks		Streaks		Streaks		Streaks		Streaks	
Homogeneously distributed		Homogeneously distributed		Homogeneously distributed		Homogeneously distributed		Homogeneously distributed		Homogeneously distributed	
Little to none		Little to none		Little to none		Little to none		Little to none		Little to none	
Diffuse clusters		Diffuse clusters		Diffuse clusters		Diffuse clusters		Diffuse clusters		Diffuse clusters	
Streaks		Streaks		Streaks		Streaks		Streaks		Streaks	
Homogeneously distributed		Homogeneously distributed		Homogeneously distributed		Homogeneously distributed		Homogeneously distributed		Homogeneously distributed	
Little to none		Little to none		Little to none		Little to none		Little to none		Little to none	
Diffuse clusters		Diffuse clusters		Diffuse clusters		Diffuse clusters		Diffuse clusters		Diffuse clusters	
Streaks		Streaks		Streaks		Streaks		Streaks		Streaks	
Homogeneously distributed		Homogeneously distributed		Homogeneously distributed		Homogeneously distributed		Homogeneously distributed		Homogeneously distributed	
Little to none		Little to none		Little to none		Little to none		Little to none		Little to none	
Diffuse clusters		Diffuse clusters		Diffuse clusters		Diffuse clusters		Diffuse clusters		Diffuse clusters	
Streaks		Streaks		Streaks		Streaks		Streaks		Streaks	
Homogeneously distributed		Homogeneously distributed		Homogeneously distributed		Homogeneously distributed		Homogeneously distributed		Homogeneously distributed	
Little to none		Little to none		Little to none		Little to none		Little to none		Little to none	
Diffuse clusters		Diffuse clusters		Diffuse clusters		Diffuse clusters		Diffuse clusters		Diffuse clusters	
Streaks		Streaks		Streaks		Streaks		Streaks		Streaks	
Homogeneously distributed		Homogeneously distributed		Homogeneously distributed		Homogeneously distributed		Homogeneously distributed		Homogeneously distributed	
Little to none		Little to none		Little to none		Little to none		Little to none		Little to none	
Diffuse clusters		Diffuse clusters		Diffuse clusters		Diffuse clusters		Diffuse clusters		Diffuse clusters	
Streaks		Streaks		Streaks		Streaks		Streaks		Streaks	
Homogeneously distributed		Homogeneously distributed		Homogeneously distributed		Homogeneously distributed		Homogeneously distributed		Homogeneously distributed	
Little to none		Little to none		Little to none		Little to none		Little to none		Little to none	
Diffuse clusters		Diffuse clusters		Diffuse clusters		Diffuse clusters		Diffuse clusters		Diffuse clusters	
Streaks		Streaks		Streaks		Streaks		Streaks		Streaks	
Homogeneously distributed		Homogeneously distributed		Homogeneously distributed		Homogeneously distributed		Homogeneously distributed		Homogeneously distributed	
Little to none		Little to none		Little to none		Little to none		Little to none		Little to none	
Diffuse clusters		Diffuse clusters		Diffuse clusters		Diffuse clusters		Diffuse clusters		Diffuse clusters	
Streaks		Streaks		Streaks		Streaks		Streaks		Streaks	
Homogeneously distributed		Homogeneously distributed		Homogeneously distributed		Homogeneously distributed		Homogeneously distributed		Homogeneously distributed	
Little to none		Little to none		Little to none		Little to none		Little to none		Little to none	
Diffuse clusters		Diffuse clusters		Diffuse clusters		Diffuse clusters		Diffuse clusters		Diffuse clusters	
Streaks		Streaks		Streaks		Streaks		Streaks		Streaks	
Homogeneously distributed		Homogeneously distributed		Homogeneously distributed		Homogeneously distributed		Homogeneously distributed		Homogeneously distributed	
Little to none		Little to none		Little to none		Little to none		Little to none		Little to none	
Diffuse clusters		Diffuse clusters		Diffuse clusters		Diffuse clusters		Diffuse clusters		Diffuse clusters	
Streaks		Streaks		Streaks		Streaks		Streaks		Streaks	
Homogeneously distributed		Homogeneously distributed		Homogeneously distributed		Homogeneously distributed		Homogeneously distributed		Homogeneously distributed	
Little to none		Little to none		Little to none		Little to none		Little to none		Little to none	
Diffuse clusters		Diffuse clusters		Diffuse clusters		Diffuse clusters		Diffuse clusters		Diffuse clusters	
Streaks		Streaks		Streaks		Streaks		Streaks		Streaks	
Homogeneously distributed		Homogeneously distributed		Homogeneously distributed		Homogeneously distributed		Homogeneously distributed		Homogeneously distributed	
Little to none		Little to none		Little to none		Little to none		Little to none		Little to none	
Diffuse clusters		Diffuse clusters		Diffuse clusters		Diffuse clusters		Diffuse clusters		Diffuse clusters	
Streaks		Streaks		Streaks		Streaks		Streaks		Streaks	
Homogeneously distributed		Homogeneously distributed		Homogeneously distributed		Homogeneously distributed		Homogeneously distributed		Homogeneously distributed	
Little to none		Little to none		Little to none		Little to none		Little to none		Little to none	
Diffuse clusters		Diffuse clusters		Diffuse clusters		Diffuse clusters		Diffuse clusters		Diffuse clusters	
Streaks		Streaks		Streaks		Streaks		Streaks		Streaks	
Homogeneously distributed		Homogeneously distributed		Homogeneously distributed		Homogeneously distributed		Homogeneously distributed		Homogeneously distributed	
Little to none		Little to none		Little to none		Little to none		Little to none		Little to none	
Diffuse clusters		Diffuse clusters		Diffuse clusters		Diffuse clusters		Diffuse clusters		Diffuse clusters	
Streaks		Streaks		Streaks		Streaks		Streaks		Streaks	
Homogeneously distributed		Homogeneously distributed		Homogeneously distributed		Homogeneously distributed		Homogeneously distributed		Homogeneously distributed	
Little to none		Little to none		Little to none		Little to none		Little to none		Little to none	
Diffuse clusters		Diffuse clusters		Diffuse clusters		Diffuse clusters		Diffuse clusters		Diffuse clusters	
Streaks		Streaks		Streaks		Streaks		Streaks		Streaks	
Homogeneously distributed		Homogeneously distributed		Homogeneously distributed		Homogeneously distributed		Homogeneously distributed		Homogeneously distributed	
Little to none		Little to none		Little to none		Little to none		Little to none		Little to none	
Diffuse clusters		Diffuse clusters		Diffuse clusters		Diffuse clusters		Diffuse clusters		Diffuse clusters	
Streaks		Streaks		Streaks		Streaks		Streaks		Streaks	
Homogeneously distributed		Homogeneously distributed		Homogeneously distributed		Homogeneously distributed		Homogeneously distributed		Homogeneously distributed	
Little to none		Little to none		Little to none		Little to none		Little to none		Little to none	
Diffuse clusters		Diffuse clusters		Diffuse clusters		Diffuse clusters		Diffuse clusters		Diffuse clusters	
Streaks		Streaks		Streaks		Streaks		Streaks		Streaks	
Homogeneously distributed		Homogeneously distributed		Homogeneously distributed		Homogeneously distributed		Homogeneously distributed		Homogeneously distributed	
Little to none		Little to none		Little to none		Little to none		Little to none		Little to none	
Diffuse clusters		Diffuse clusters		Diffuse clusters		Diffuse clusters		Diffuse clusters		Diffuse clusters	
Streaks		Streaks		Streaks		Streaks		Streaks		Streaks	
Homogeneously distributed		Homogeneously distributed		Homogeneously distributed		Homogeneously distributed		Homogeneously distributed		Homogeneously distributed	
Little to none		Little to none		Little to none		Little to none		Little to none		Little to none	
Diffuse clusters		Diffuse clusters		Diffuse clusters		Diffuse clusters		Diffuse clusters		Diffuse clusters	
Streaks		Streaks		Streaks		Streaks		Streaks		Streaks	
Homogeneously distributed		Homogeneously distributed		Homogeneously distributed		Homogeneously distributed		Homogeneously distributed		Homogeneously distributed	
Little to none		Little to none		Little to none		Little to none		Little to none		Little to none	
Diffuse clusters		Diffuse clusters		Diffuse clusters		Diffuse clusters		Diffuse clusters		Diffuse clusters	
Streaks		Streaks		Streaks		Streaks		Streaks		Streaks	
Homogeneously distributed		Homogeneously distributed		Homogeneously distributed		Homogeneously distributed		Homogeneously distributed		Homogeneously distributed	
Little to none		Little to none		Little to none		Little to none		Little to none		Little to none	
Diffuse clusters		Diffuse clusters		Diffuse clusters		Diffuse clusters		Diffuse clusters		Diffuse clusters	
Streaks		Streaks		Streaks		Streaks		Streaks		Streaks	
Homogeneously distributed		Homogeneously distributed		Homogeneously distributed		Homogeneously distributed		Homogeneously distributed		Homogeneously distributed	
Little to none		Little to none		Little to none		Little to none		Little to none		Little to none	
Diffuse clusters		Diffuse clusters		Diffuse clusters		Diffuse clusters		Diffuse clusters		Diffuse clusters	
Streaks		Streaks		Streaks		Streaks		Streaks		Streaks	
Homogeneously distributed		Homogeneously distributed		Homogeneously distributed		Homogeneously distributed		Homogeneously distributed		Homogeneously distributed	
Little to none		Little to none		Little to none		Little to none		Little to none		Little to none	
Diffuse clusters		Diffuse clusters		Diffuse clusters		Diffuse clusters		Diffuse clusters		Diffuse clusters	
Streaks		Streaks		Streaks		Streaks		Streaks		Streaks	
Homogeneously distributed		Homogeneously distributed		Homogeneously distributed		Homogeneously distributed		Homogeneously distributed		Homogeneously distributed	
Little to none		Little to none		Little to none		Little to none		Little to none		Little to none	
Diffuse clusters		Diffuse clusters		Diffuse clusters		Diffuse clusters		Diffuse clusters		Diffuse clusters	
Streaks		Streaks		Streaks		Streaks		Streaks		Streaks	
Homogeneously distributed		Homogeneously distributed		Homogeneously distributed		Homogeneously distributed		Homogeneously distributed		Homogeneously distributed	
Little to none		Little to none		Little to none		Little to none		Little to none		Little to none	
Diffuse clusters		Diffuse clusters		Diffuse clusters		Diffuse clusters		Diffuse clusters		Diffuse clusters	
Streaks		Streaks		Streaks		Streaks		Streaks		Streaks	
Homogeneously distributed		Homogeneously distributed		Homogeneously distributed		Homogeneously distributed		Homogeneously distributed		Homogeneously distributed	
Little to none		Little to none		Little to none		Little to none		Little to none		Little to none	
Diffuse clusters		Diffuse clusters		Diffuse clusters		Diffuse clusters		Diffuse clusters		Diffuse clusters	
Streaks		Streaks		Streaks		Streaks		Streaks		Streaks	
Homogeneously distributed		Homogeneously distributed		Homogeneously distributed		Homogeneously distributed		Homogeneously distributed		Homogeneously distributed	
Little to none		Little to none		Little to none		Little to none		Little to none		Little to none	
Diffuse clusters		Diffuse clusters		Diffuse clusters		Diffuse clusters		Diffuse clusters		Diffuse clusters	
Streaks		Streaks		Streaks		Streaks		Streaks		Streaks	
Homogeneously distributed		Homogeneously distributed		Homogeneously distributed		Homogeneously distributed		Homogeneously distributed		Homogeneously distributed	
Little to none		Little to none		Little to none		Little to none		Little to none		Little to none	
Diffuse clusters		Diffuse clusters		Diffuse clusters		Diffuse clusters		Diffuse clusters		Diffuse clusters	
Streaks		Streaks		Streaks		Streaks		Streaks		Streaks	
Homogeneously distributed		Homogeneously distributed		Homogeneously distributed		Homogeneously distributed		Homogeneously distributed		Homogeneously distributed	
Little to none		Little to none		Little to none		Little to none		Little to none		Little to none	
Diffuse clusters		Diffuse clusters		Diffuse clusters		Diffuse clusters		Diffuse clusters		Diffuse clusters	
Streaks		Streaks		Streaks		Streaks		Streaks		Streaks	
Homogeneously distributed		Homogeneously distributed		Homogeneously distributed		Homogeneously distributed		Homogeneously distributed		Homogeneously distributed	
Little to none		Little to none		Little to none		Little to none		Little to none		Little to none	
Diffuse clusters		Diffuse clusters		Diffuse clusters		Diffuse clusters		Diffuse clusters		Diffuse clusters	
Streaks		Streaks		Streaks		Streaks		Streaks		Streaks	
Homogeneously distributed		Homogeneously distributed		Homogeneously distributed		Homogeneously distributed		Homogeneously distributed		Homogeneously distributed	
Little to none		Little to none		Little to none		Little to none		Little to none		Little to none	
Diffuse clusters		Diffuse clusters		Diffuse clusters		Diffuse clusters		Diffuse clusters		Diffuse clusters	
Streaks		Streaks		Streaks		Streaks		Streaks		Streaks	
Homogeneously distributed											

cause they reduce imaging signal and contrast, and they also interfere with X-ray imaging.

2.2 Sample Storage

Clinker specimens are moisture-sensitive so storage in a desiccator when not in use is necessary. Some hydration of the more reactive constituents (free lime) will inevitably occur, necessitating sample examination as soon as practical after preparation is complete. Hydration of free lime may also reflect sample storage-related prehydration and may be a useful observation relevant in understanding anomalous cement behavior. The prehydration features may be distinguished by their surface being level with the specimen whereas hydration after specimen preparation will stand in high relief due to the substantial volume increase.

2.3 SEM Imaging

High-quality images for quantitative analysis can be obtained with the following SEM operating conditions:

1. 12 kV accelerating voltage,
2. 2 nA to 4 nA probe current, adjusted to keep a relatively high X-ray count rate with minimal dead time,
3. a scan rate of 5 min/frame for an image size of 1024 pixels \times 768 pixels to minimize BE noise,
4. an accumulation of about 15 frames to improve the definition of the X-ray images
5. A magnification of 300 \times , which provides a spatial resolution of approximately 1.0 μm /pixel, which is typically on the order of the width of the beam's interaction with the specimen.

These settings are a useful starting point to obtain useful images, and are judged to represent a balance between fast collection times, a match in resolution of BE images with X-ray maps, and instrument stability.

The local brightness in a BE compositional image is proportional to the average atomic number, \bar{Z} , of the phase in that location, and the XR image reflects element spatial distribution over the same field of view. The backscatter coefficient, η , is a measure of the backscattered electron fraction and, following Goldstein *et al.* [8], is estimated using the mass fractions and η values for each constituent. Table 1 lists phases found in clinker and cement in descending order of their backscattered coefficient and gray intensity. Caution is necessary here because the brightness ranking may change depending upon chemistry variability due to impurities; the exact values are not as important as the general ranking of the phases in the table. The identification of the individual phases also includes supplemental information such as domain shape (*e.g.*, angular or rounded), position within the microstructure (*e.g.*, framework grain, matrix, dispersed phase), and bulk chemistry as described in Table 2.

Table 1: Clinker phases, compositions, densities, average atomic number, and backscattered electron coefficient ranked according to relative SEM BE image brightness [17].

Phase	Composition	Notation	Density (Mg m^{-3})	\bar{Z}	η
Ferrite	$\text{Ca}_2(\text{Al}_x\text{Fe}_{1-x})_2\text{O}_5$	C_4AF	3.77	16.65	0.1860
Free lime	CaO	C	3.32	16.58	0.1882
Alite	Ca_3SiO_5	C_3S	3.13 to 3.22	15.06	0.1716
Belite	Ca_2SiO_4	C_2S	3.28 to 3.31	14.56	0.1662
Arcanite	K_2SO_4	$\text{K}\bar{\text{S}}$	2.67	14.41	0.1652
Aluminate-c ^a	$\text{Ca}_3\text{Al}_2\text{O}_6$	C_3A	3.04	14.34	0.1639
Aluminate-o ^b	$\text{Ca}_3\text{Al}_2\text{O}_6$	C_3A	2.56	13.87	0.1588
Aphthitalite	$\text{NaCaAl}_3\text{O}_9$	NCA	2.7	13.69	0.1577
Thenardite	Na_2SO_4	$\text{N}\bar{\text{S}}$	2.66	10.77	0.1249
Periclase	MgO	M	3.58	10.41	0.1213

^a cubic polymorph

^b orthorhombic polymorph

The BE contrast between alite and belite is relatively strong, but that between belite and cubic tricalcium aluminate is generally too low to rely on contrast to distinguish them. For such phase pairs that have similar BE coefficients, or for phases that have BE coefficients too low to be resolved in the BE image, XR imaging is used to distinguish them based on their composition. For example, periclase and some alkali sulfates often appear black, like the epoxy-filled voids, because of the brightness and contrast settings necessary to make the other phases distinct. Combining the XR and BE images facilitates their discrimination much better than relying on either image alone. Information redundancies also occur that should be reduced or eliminated to improve the phase distinction. For example, the Ca and Si XR image, or a ratio of the two, may be considered for distinguishing the calcium silicate phases. The BE image, however, provides a much better distinction between the calcium silicates and is preferred because of it is less “grainy” than the XR image. Further details and examples of how SEM images may be combined to render these phases distinct will be shown in a later section.

2.4 X-Ray Microanalysis and Imaging

X-Rays are produced as a result of the interaction of the electron beam with the specimen, and they are typically displayed as a set of peaks with a continuous background (Fig. 3). The energy-dispersive X-ray analyzer (EDX) ranks and counts X-rays based upon their energy. The spectrum from alite shown in Fig. 3 has the characteristic peaks for calcium, silicon, aluminum, magnesium, sodium, oxygen, and carbon (the conductive coating), and a background. The concentrations of the elements can be quantified if suitable standards are available, and are typically expressed as mass percent of the oxide.

Table 2: Textural and chemical characteristics useful for distinguishing clinker phases.

Phase	Identifying Characteristics
Free Lime	Bright BE, rounded crystals, sometimes clustered, strong Ca and no Fe
Ferrite	Bright BE, dendritic to prismatic matrix phase, high Ca, medium Fe and Al
Alite	Medium-high BE, euhedral to anhedral crystals, framework grain, strong Ca and Si, minor Mg and Al.
Belite	Medium BE, rounded crystals, framework grain, strong Ca and Si, minor Mg, Al, and weak S. Sometimes clustered.
Aluminate	Medium BE, fine to lath-like crystals, matrix phase between ferrite crystals, Ca, Al, Mg, K, Fe and sometimes Na.
Arcanite	Medium BE, crystals dispersed, typically along boundaries of matrix and framework grains, high K, S
Aphthitalite	Low BE, crystals dispersed, typically along boundaries of matrix and framework grains, high K, Na, S
Thenardite	Low BE, crystals dispersed, typically along boundaries of matrix and framework grains, high Na, S
Periclase	Low BE, equant to dendritic grains, clustered to dispersed

3 Application to SRM 2686a

This section demonstrates the use of the foregoing procedures for analyzing the NIST Standard Reference Material (SRM) clinker 2686a [15]. A representative BE image of this clinker is shown in Fig. 4, and all subsequent images in this section will use the same image field for illustration purposes. The phase domains in this clinker have an intermediate size compared to the other SRM clinkers. The spatial distribution of phases is heterogeneous, and little free lime is detected. Alite occurs as subhedral to anhedral crystals approximately 30 μm in size. Belite occurs in large clusters with an approximate crystal size of 20 μm . The matrix is differentiated with a medium-to fine-grained lath-like ferrite, and fine-grained aluminate filling the inter-lath voids. Equant periclase crystals up to 15 μm are common throughout the microstructure and the alkali sulfate phases aphthitalite and arcanite are distributed throughout the microstructure. According to the Hofmänner diagnostic chart in Fig. 2, the belite clustering represents heterogeneity or over-sized silica grains in the raw mix. The fine-grained matrix indicates rapid cooling from 1300 °C, and the slightly elevated belite content may reflect a slightly low CaO content.

An annotated BE image of this clinker is shown in Fig. 4, illustrating the distinct contrasts be-

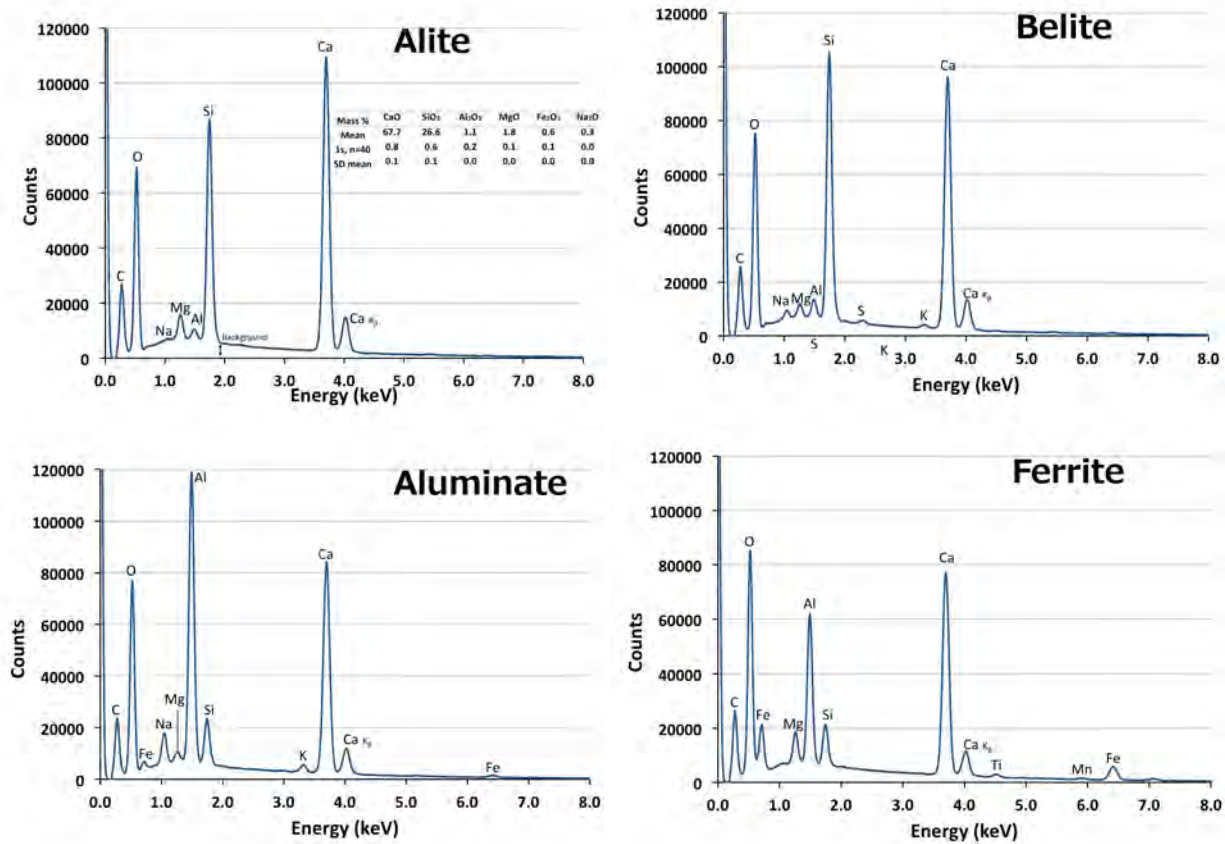


Figure 3: Energy-dispersive X-ray microanalysis shows spectra from the primary clinker phases exhibit characteristic spectra on a continuous background and standard-based quantitative analysis of chemical composition expressed as oxides.

tween most of the phases. Reference to Tables 1 and 2 should allow one to identify the constituent phases. While the contrast between belite and aluminate is not distinguishable, as mentioned in the previous section, they are still texturally distinct and can be distinguished on this basis even within the BE image, the belite being a large-grained framework grain and the aluminate being a fine-grained matrix. Periclase and alkali sulfates appear dark, like the voids, although they would be easier to detect with a brighter image setting. The ancillary XR images for the major elements will be used to identify the locations of these phases as well as isolate them in the image processing stage.

This image set was collected at 1200 \times magnification using a 1024 pixel \times 768 pixel image, producing a spatial resolution of 2 μ m/pixel. This is in excess of that used for routine imaging and was done here to better illustrate the phases. The set of XR images associated with this backscattered electron image is shown in Fig. 5. These images were collected simultaneously

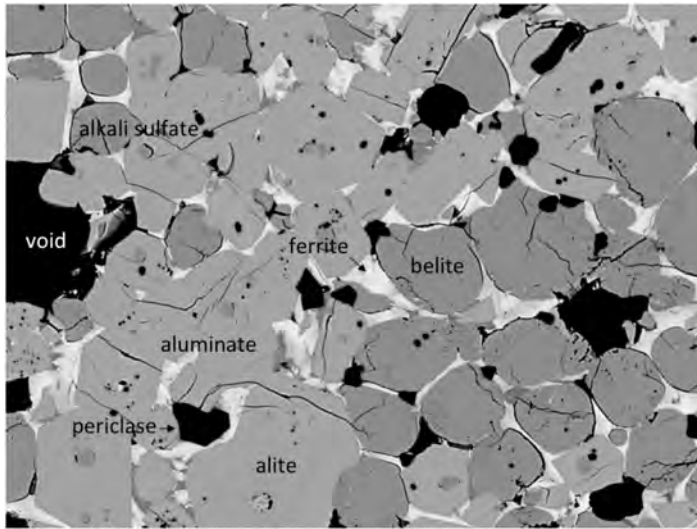


Figure 4: SEM backscattered electron image of SRM 2686a, showing a medium-grained, heterogeneous silicate distribution and a coarse-grained matrix with phase identifications. Field width is 256 μm .

so they are registered, with the same pixels on each image representing the same region. The brightness is proportional to X-ray counts, and roughly proportional to element concentration. While the figure is displayed as a gray-scale image, pseudo-coloring can sometimes improve the visualization of the element distribution. The images in Fig. 5 have been modified to remove contributions from the continuous spectrum background using a simple subtraction routine that will be described more fully in the next section.

The energy-dispersive X-Ray signal consists of the characteristic spectrum for each element and a continuous spectrum, often called the background (Fig. 3). This background will contribute image noise that may be significant, especially for 8-bit image formats that can resolve only 256 gray levels. A 16-bit image format, with 65 536 gray levels, can offer a better signal-to-noise ratio. In other cases, low concentrations of an element are expressed as a very weak and variable signal, given the relatively short X-ray imaging dwell time. While these low-concentration elements are helpful for quantitative microanalysis of clinker mineral compositions, they are not as useful for phase segmentation, and are another example of redundancy.

The differences between the silicates, alite and belite, are shown in the BE image (Fig. 4). The differences in concentration of Ca and Si in the associated XR images (Fig. 5) reflects the different Ca and Si concentrations of alite and belite.

The aluminum and iron images in Fig. 5 highlight the interstitial (matrix) phases, aluminate and ferrite³. These elements also exist in low concentrations in some of the other phases, and will therefore have low counts throughout other portions of their XR images. The iron image is another example of an image redundancy because it highlights mainly the ferrite and, to a lesser

³For brevity, tricalcium aluminate is routinely designated simply as “aluminate,” distinguished as cubic or orthorhombic where appropriate, and tetracalcium aluminoferrite is designated as “ferrite”.

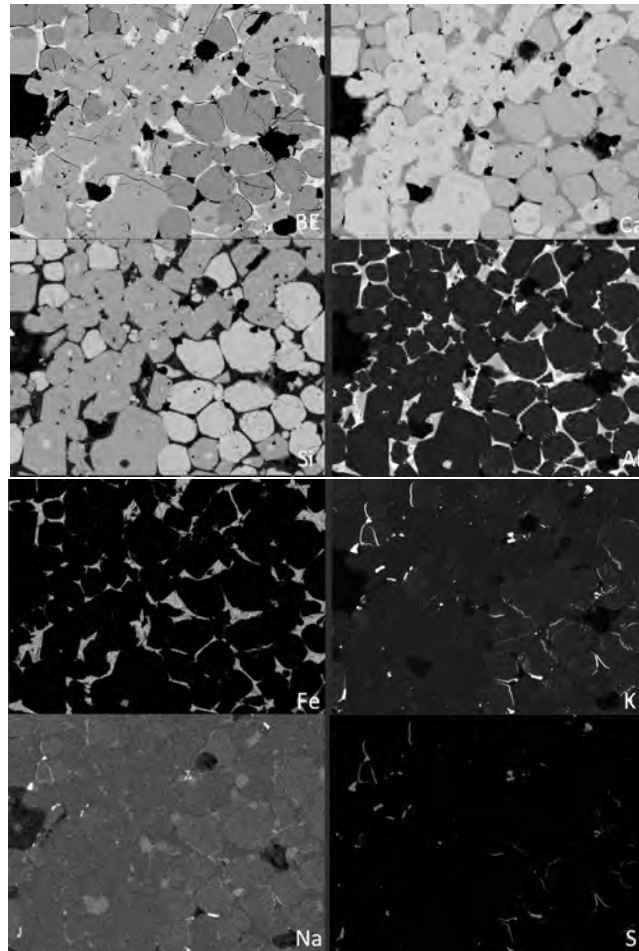


Figure 5: X-ray microanalysis images of the spatial distribution of elements for the field of view shown in Figure 4. The image in the upper left is the BE image. Field width is 256 μm .

degree, the aluminate phase. These phases are better distinguished in the BE image (Fig. 4) and, for aluminate, the BE and the Al image, so the iron image is not used for the image processing. The aluminum XR image, however, is important because it can be used together with the BE image to distinguish belite from aluminate based on the high concentration of Al the latter phase. Further features that stand out upon a cursory scan of Fig. 5 are periclase crystals dispersed throughout the image (regions of high Mg), arcanite (areas with strong signals from both S and K), and aphthitalite (regions with S, K, and Na).

For a more systematic exploration of the phase constituents and their distribution in the clinker, the first step is to examine the individual and then combinations of the image set. This is accomplished using ImageJ [10], or a similar image viewer, and merging different image combinations. Two combinations can generally serve to highlight all the phases. These combinations may also be used to see if a particular image improves or confounds a phase distinction, allowing the user to decide on adding that image to the set that will be used for the image processing used

to uniquely identify the clinker phases. ImageJ can merge up to seven images while most other codes display three, as a red, a green, and a blue color plane (RGB). Displaying the BE image, Mg, and Al as a RGB image allows distinction of alite, belite, ferrite, aluminate, periclase, and voids. Displaying the BE image with K and Na provides distinction of the alkali sulfates. This process will be discussed in more detail in a later section.

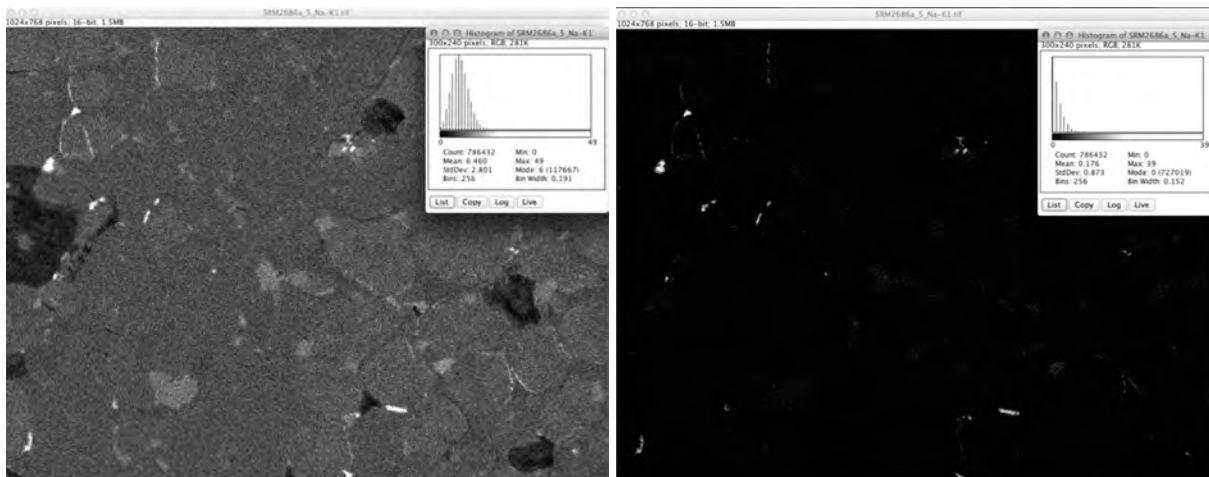


Figure 6: Reducing noise associated with the continuous spectrum background improves the delineation of aphtthitalite from the raw Na XR image (left) and histogram, as shown in the processed subtracted image (right). Field width is 256 μm .

3.1 Image Processing

The next four sections provide detailed guidance for processing the experimentally obtained images and transforming them to a single phase segmented image suitable for quantitative stereological analysis. The Appendix provides a condensed set of instructions distilled from this discussion.

As an example applied to SRM 2686a, Fig. 6 shows the Na XR map associated with one field of view. In this image, the continuous background and inherently low counts associated with aphtthitalite are problematic for segmentation decisions, because they reduce the signal-to-noise ratio relative to that in an image with a greater element concentration. The background count level can be determined from the histogram (see the insets of Fig. 6), or by reading the counts while scrolling the pointer across the background; the Na image in Fig. 6 registers about 10 counts. Once the background count level is determined, the background can be subtracted. To do so within ImageJ, choose the *Process*→*Math*→*Subtract* operation. This operation opens a preview option window where the subtraction threshold value can be entered (10, in this case). The resulting image, shown as the right image in Fig. 6, more clearly distinguishes the aphtthitalite domains.

The Mg XR map for the same field of SRM 2686a shows the spatial distribution of Mg in the silicates, the matrix, and, in particular, periclase (Fig. 7). The silicates and matrix phases

are more clearly distinguished using a combination of the BE image and Al XR image, so the Mg distribution information is not needed for their segmentation. The low concentration distribution of Mg becomes apparent in the Mg image by expanding the brightness and contrast (Fig. 7, left). Just as for the Na distribution, removal of the low-concentration and background counts from the Mg map produces a clearer delineation of the Mg distribution for periclase. In this case, scrolling the pointer over the low-Mg phases, such as alite, in the upper image of Fig. 7 indicates the maximum background level to be about 20 counts, so 20 can be used as the threshold value in ImageJ's *Process*→*Math*→*Subtract* operation to produce the right image in Fig. 7.

ImageJ has other operations in its *Image*→*Noise* menu for removing additional image artifacts (e.g., speckling) that can complicate phase segmentation decisions. Examples include *Despeckle* and *Remove Outliers*.

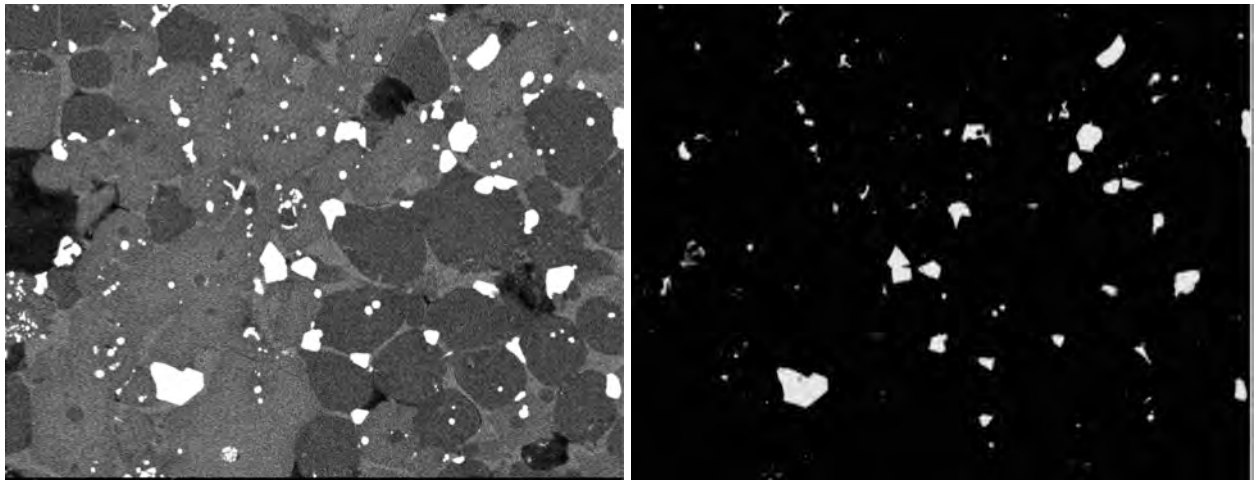


Figure 7: Mg XR map associated with low concentrations in the silicates and matrix phases may confound segmentations. Subtracting low-level signal associated with background and low concentrations of Mg presents a clearer rendering of periclase location. Field width is 256 μm .

Smoothing filters, several of which are available in ImageJ can improve the distinction between phases, but selecting one that preserves edge detail is important to preserve the texture of the clinker microstructure. A useful ImageJ filter is called *Thresholded Blur* [20], which features an interactive, selective mean filter and displays an image preview to assess the effect of the filter's settings prior to committing it. Used carefully, this filter will enhance distinction between phases by reducing noise and retaining edge definition. It will later be important for cleaning up incorrectly assigned pixels after the segmentation is complete. Figs. 8 and 9 show examples of the application of the Thresholded Blur algorithm to the BE image and the Ca XR image, respectively. The BE image exhibits the lowest noise of the set, although there can be some variability in gray intensity and minor scratches that may appear slightly darker than the surroundings. These minor imperfections can be removed by careful selection of smoothing settings. In Fig. 8, image set (A) is the original BE image, including fine scratches; a magnified portion is shown at the bottom of the figure. The smoothed image (B) in Fig. 8 shows a much more uniform gray for

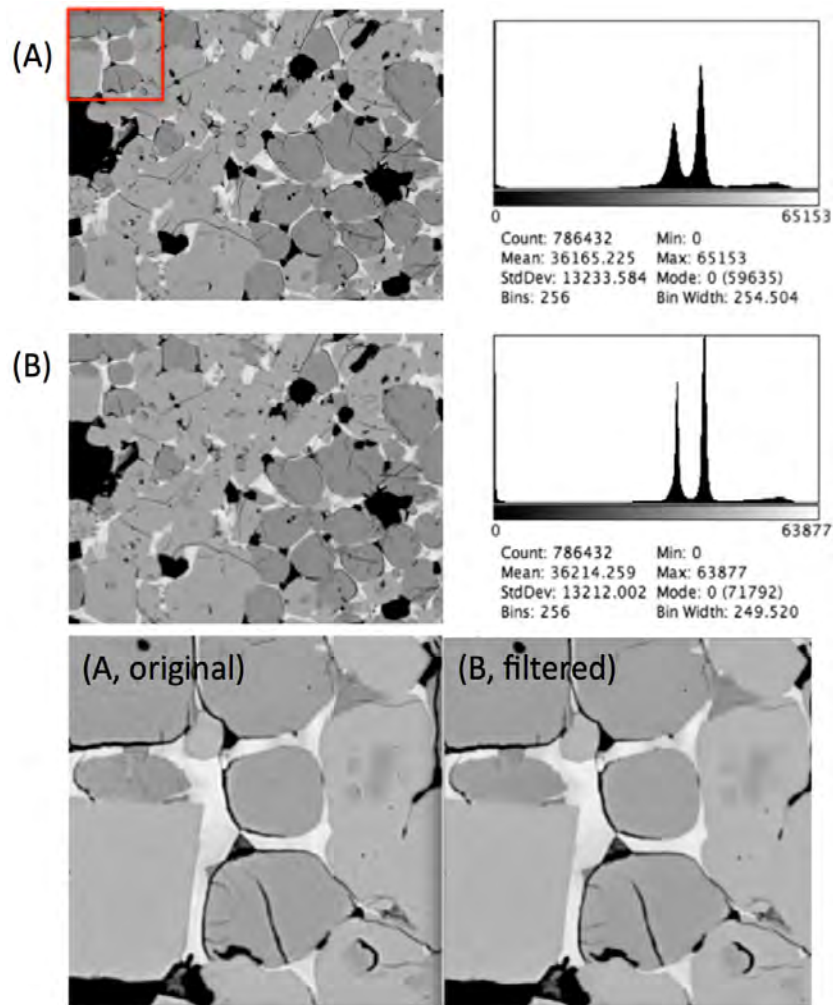


Figure 8: Thresholded blur filter applied to the BE image removes minor scratch marks and makes the gray levels for each phase more uniform as seen in the images and gray level histograms. Field width is 256 μm .

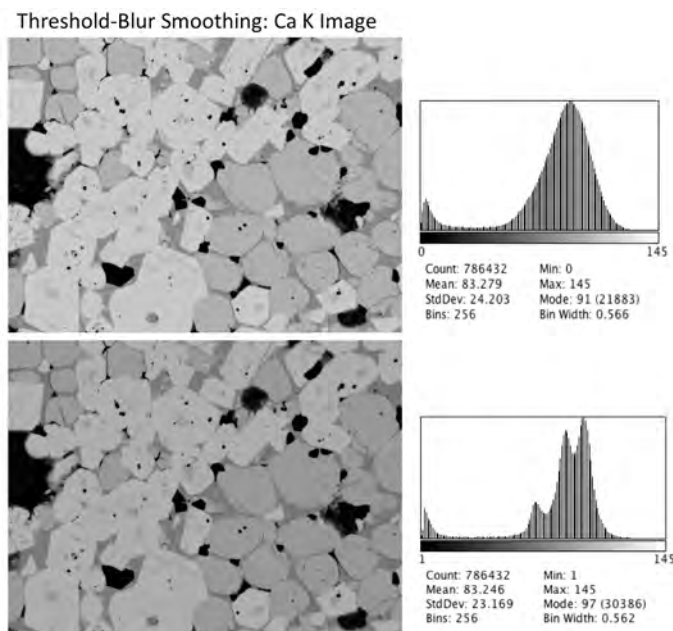


Figure 9: Thresholded Blur algorithm applied to the Ca X-ray image improves the distinction between phases by comparing gray level histograms from the initial (A) and filtered (B) images, which now shows distinct peaks for alite, belite and matrix. Field width is 256 μm .

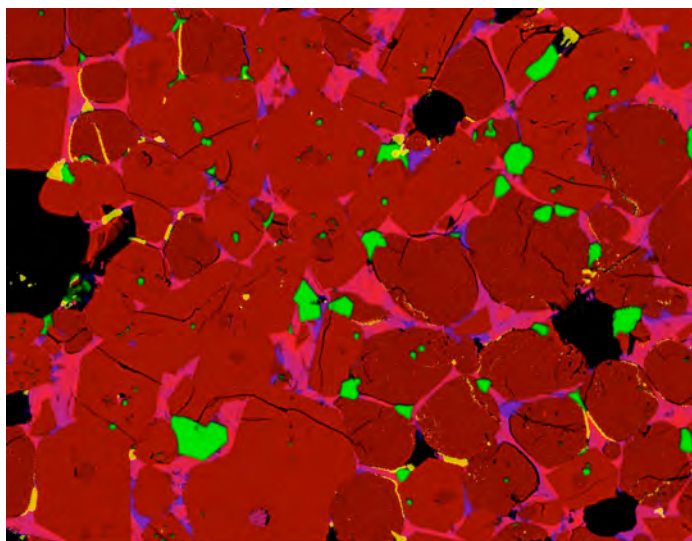


Figure 10: Composite image with the BE as red, Mg as green, Al as blue and S as yellow illustrates how the addition of the X-ray data improves phase identification. Alite is a brighter red than belite, the matrix phases are bluish (aluminates) and pink (ferrite), periclase is green, and alkali sulfates are yellow. Field width is 256 μm .

each phase, with the finer scratches removed while retaining the grain boundaries, and providing an improved distinction between the silicate histogram peaks. The smoothing settings that produced Fig. 8 (B) included a kernel radius of 2 pixels, an intensity threshold of 10, a softness of 0, and strength of 2. These values were selected based on the description of their functions [10] and the effects on smoothing the image without loss of phase definition.

3.2 Visualizing Phase Occurrence and Distribution by Color Merge

The *Color Merge* operation in ImageJ is a useful tool to visualize and identify the phases and their spatial distribution. This operation combines, or stacks, BE and XR images while assigning unique colors to each image. The colors blend and, depending upon the image combination chosen, highlight the different phases. This is best done with a subset of the XR images or with XR images and the BE image. The important images to combine include the BE, Mg, Al, K, Na, and S. Other images either do not further aid in phase discrimination (e.g., Ca, Si) or have such low concentrations that their noise confounds the phase segmentation (e.g., Ti, Mn).

The color merge is accomplished in ImageJ using the *Image→Color→Merge Channels* operation. Depending on the version of ImageJ, up to seven images can be merged at once. Fig. 10 shows the merging of the BE (red), Mg (green), Al (blue), and S (yellow). Arcanite and aphthitalite could be distinguished from each other by adding the K and Na images to the merge. The aluminum XR image makes the distinction between belite and aluminate clear, even though their contrast in the BE image is nearly the same. The Mg image reveals the locations of periclase, while the S image highlights the alkali sulfates. Alkali sulfate phases in Fig. 10 are evident at grain boundaries and within fractures of the belite crystals, which are typical locations for these phases. Simpler image combinations than those in Fig. 10, such as BE-Mg-Al and BE-Na-K, can be useful for identifying phases, especially if the image display code can show only three color planes.

With the visualization of the phases and their distribution as in Fig. 10, the next step in quantitative image analysis is to train the segmentation routine to recognize the individual phases and then generate an indexed image in which each phase is uniquely identified and coded. This process involves classification of each pixel as the phase to which it most likely belongs, based upon a user-created training set and multispectral image processing.

Based on the exploratory analysis using ImageJ and the color merging operations illustrated in Fig. 10, a minimum set of images selected to discriminate each phase are included in the segmentation operations. This set typically includes BE, Al, Mg, K, Na, and S. As mentioned previously, other element images should not be included because they do not add any new information to the image set, and may even confound the segmentation. More details on the data collection, the multi-spectral image processing, and analysis are given elsewhere [12, 19].

3.3 Image Processing with MultiSpec

MultiSpec, a software package developed at Purdue University, is a processing system for interactively analyzing multispectral image data [14]. It is used here to generate the final segmented

image from a small subset of images described in the previous section. A condensed set of instructions for using ImageJ and MultiSpec can be found in the Appendix. This section provides a summary of the steps required to compile a data set, establish the training fields, classify, and generate the segmented, indexed image for final analysis.

MultiSpec has tools to help establish an optimal data set for analysis, but the relative simplicity of the phase chemistry and image sizes make this a relatively straightforward task that can be efficiently completed with ImageJ's Color Merge operation described earlier. The less useful X-ray images can optionally be included, but they should be placed as the last of the images so that they can be easily excluded from the classification if necessary.

MultiSpec identifies and reports the image size, bit depth, and number of planes (RGB color or single gray). In most cases, the default parameters suggested by the software can be accepted. In some cases when processing is performed, an option is available to write a text file with the details and a processed image file; such cases will be noted in the following description.

Processing clinker or cement microstructure images with MultiSpec involves seven basic steps:

1. Load the BE image
2. Link the BE image to the XR image set
3. Rectify and save the linked files
4. Identify phases (class assignment)
5. Set up training fields
6. Perform phase segmentation and check its quality
7. Save the MultiSpec project

Step 1: Load the BE image. Fig. 11 shows how to load the BE image as a multispectral type using the *File*→*Open Image* menu item and selecting the multispectral option. Under the “Multispectral Display Specifications” section of the dialog, the defaults can all be accepted with the exception of the “Enhancement” section; here one will usually opt to leave the image unchanged since background noise was removed using the ImageJ *Process*→*Math*→*Subtract* function, but the image can also be clipped on the low and high end, or user selected clipping based upon a percentage of the gray level.

Step 2: Link BE and XR image sets. XR images that previously have been deemed useful in making a segmentation must be linked to the loaded BE image using the *File*→*Open Image* menu item, as shown in Fig. 12. Select the (already-modified and optimized) XR images by clicking on them individually, and check the box or drop-down menu for each new file to indicate “Link to active image window”. Deciding on a standardized image sequence is helpful to later recall the

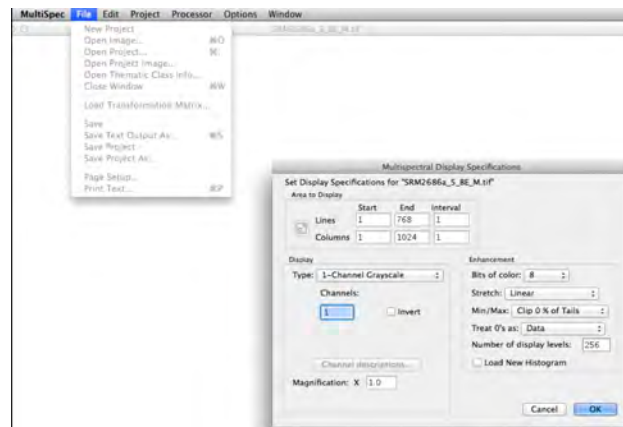


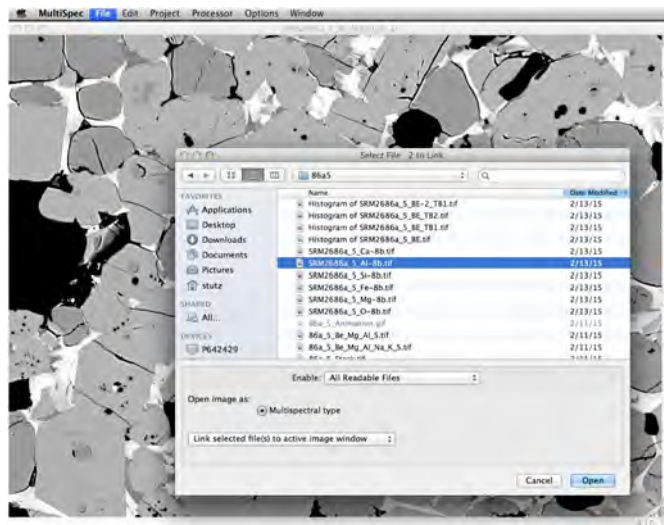
Figure 11: Loading the SEM BE image in MultiSpec interprets the image file details with an enhancement option to trim a percentage of the high- and low-end signal, if necessary.

exact image source in the virtual linked files (BE, Al, Mg, K, Na, S). These linked images can be named individually later if necessary. Any image in the sequence can also be excluded if it is later determined to hinder the classification of phases. As already stated, image exclusion is easier if the potentially problematic XR images are placed at the end of the linked image sequence. Click on the *Cancel* button to complete the linking.

Step 3: Rectify and save linked files. Use the *Processor*→*Reformat*→*Rectify Image* menu item, shown in Fig. 13, to rectify the linked files. Options are provided to subsample, translate, and rotate the images, although this is rarely needed because the SEM image set should already be suitably registered. However, if beam charging caused the BE image to be misaligned relative to the XR image set, these options can help resolve the discrepancy. The default values of the other parameters can be accepted. The *Processor*→*Reformat*→*Add Channel Descriptions* option allows one to add a descriptive name for each channel, which can be useful for keeping track of image sets that use nonstandard image sequences. Provide a file name with a .LAN extension and, before saving, check that the path is correct because it may not default to the original folder. A good practice is to use the original file name and keep everything together together in a folder of the same name. **Note:** Using a .LAN extension on the file name is important; without the .LAN extension MultiSpec will not automatically recognize the file as valid for any subsequent loading in the next steps.

Step 4: Assign classes. Reload the .LAN image set using the *File*→*Open Image* menu item (Fig. 14). If it is not highlighted as a readable file, designate the file type as “Multispectral Image Files” section of the dialog window.

Once the image set is opened, a window labeled “Multispectral Display Specifications” will appear (Fig. 15) where channel colors can be assigned (R G B), image enhancements such as clipping or transformation can be made, and image sets can be subsampled by lines and rows. This display tool functions much like the Color Merge operation in ImageJ, but it allows only



MultiSpecLink

Figure 12: Linking the BE image to a set of XR images from the same field of view is accomplished in MultiSpec by selecting each XR image, specifying “Link selected file(S) to active image window” in the drop-down menu, and completed by selecting *Cancel*.

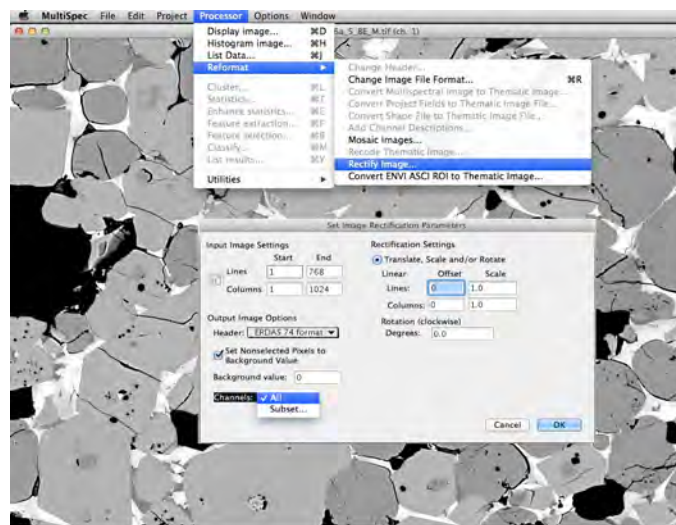


Figure 13: Saving the linked BE and X-ray images using the *Processor*→*Reformat*→*Rectify* provides a chance to subsample the set and repair any image registration issues (rectification).

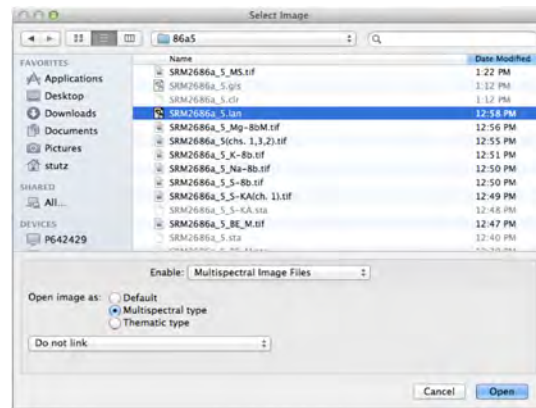


Figure 14: Selecting the linked, rectified multispectral image set, indicated by file extension .LAN will allow display of the image set and establishing training fields.

three color planes. The three-color limitation may seem restrictive, but it reduces the likelihood of confusion in interpreting the displayed images.



Figure 15: Three-color (RGB) display by channel will provide a rendering of phase distribution for the next step of establishing the training fields.

When assigning channel colors in the “Multispectral Display Specifications” window, choose channel/color combinations that will provide a clear rendering of the phase distribution. The most useful for clinker is the combination of BE (Red), Mg (Green), Al (Blue), which can clearly reveal alite, belite, aluminate, ferrite, periclase, lime, and void, as shown in the left image of Fig. 16. To complement such a color scheme, alkali sulfates can be readily identified with the combination of BE (Red), K or Na (Green) and S (Blue), as shown in the right image of Fig. 16. Often the Na image is redundant with K, but in this example there are differences representing two distinct alkali sulfate phases. This second color combination is useful because alkali sulfates are difficult to perceive from the BE image alone. The BE coefficient for arcanite is close to that of belite, and aphtitalite’s BE coefficient is low enough that it may be mistaken for void space without the additional X-ray information from the Na image.

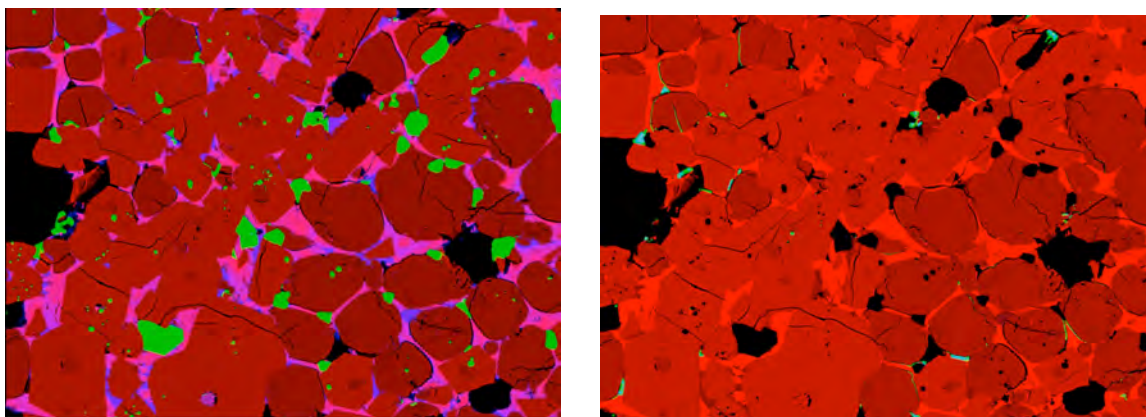


Figure 16: MultiSpec *Image→Display* allows three channels to be assigned to Red-Green-Blue color planes to facilitate identification of phase type and distribution. The upper image is BE (red), Mg (green), and Al (blue) while the lower is BE (red), K (green), and Na (blue). Field width is 256 μm .

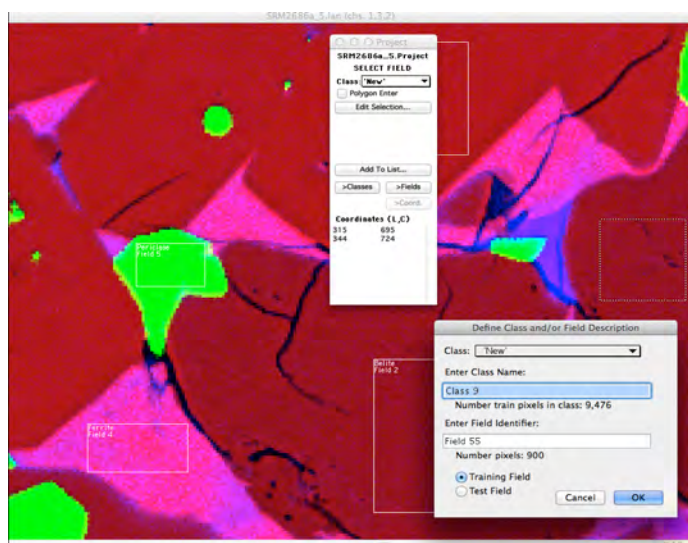


Figure 17: Training fields are defined by boxing regions typical for each phase (class) and assigning a class name. Additional training fields are created by selecting a phase, boxing a new region, and adding it to the class.

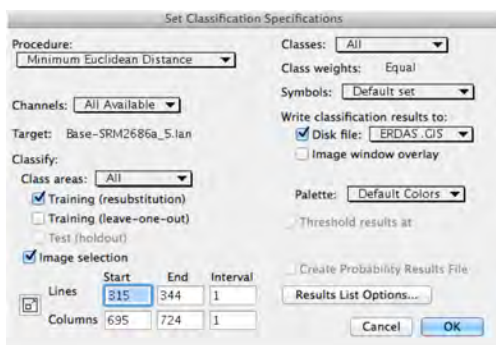


Figure 18: Classification is initiated by selection of a procedure, the use or exclusion of some image channels, and writing the classification results to a disk file.

Step 5: Establish training fields. When all the phases are identified as in Fig. 16, training fields must be assigned to condition MultiSpec for the image segmentation step.⁴ A powerful feature of MultiSpec is its ability to establish training classes by interactively highlighting regions of the image that are associated with specific phases. To set up the training classes, use *Processor*→*Statistics*, and accept the defaults in the “Set Project Options” dialog window. With the recommended image combinations to highlight the phases from the previous step, regions for each phase (or class) can be designated as shown by the white outlined boxes in Fig. 17.

The “New Project” window shows a Class Designation at the top, with ‘New’ as the default. A list of classes can be initiated here by boxing in a region in the image (mouse click and drag) across each phase individually. For each phase, the class is then added by clicking the “Add to List” button and providing a name (e.g., alite, belite). The definition of class characteristics improved as more pixels are added to the training sets. Therefore, the largest possible box ordinarily should be selected for each phase. If the box accidentally covers an unwanted area, recreate the box before selecting “Add to List”. An option is available for selecting polygonal regions instead of boxes, by clicking on line segments until the polygon is closed, but the box approach works quickly and is usually sufficient for defining classes. If a field appears to be incorrectly assigned after being added, it can be deleted before continuing by selecting class and then field in the project window to get a list of individual fields. Select the field you wish to delete and from Edit in the top command bar, select “Cut Field” to delete.

Classes will have an associated index value that is assigned based on the order in which the fields were added to the list in the Project window. A given class also optionally can be refined further into subclasses. For example, a generic alkali sulfate class could contain subclasses for arcanite and apthitalite, although a generic class is rarely helpful in phase segmentation. The important point is to use a consistent sequence to facilitate phase identification and further quantitative analysis of the indexed image. The following convention is highly recommended:

⁴MultiSpec has a built-in automated segmentation utility, which ordinarily would eliminate the need for training classes described here. However, we have found that MultiSpec’s automated segmentation utility yields less thorough, less accurate segmentations than can be obtained by establishing training classes.

1 = alite	2 = belite	3 = aluminate	4 = ferrite
5 = periclase	6 = arcanite	7 = apthitalite	8 = void

The index assignments should be recorded for later use. If phases are absent, the index values shift down accordingly. For example, if a clinker has no identifiable periclase, then the indices for arcanite, apthitalite, and void would all decrease by one.

Step 6: Segment phases. Use the *Processor*→*Classify* command to begin the image segmentation algorithm. Seven classification procedures are available in MultiSpec, and it is relatively easy to test them all to determine which one yields the best segmentation. The classification window is shown in Fig. 18. In general, both the “Minimum Euclidean Distance” and the “Fisher Linear Likelihood” algorithm work well for segmenting clinker or cement images. The results are saved by checking the “Disk File” radio button under the “Write Classification Results” section of the window. Prior to saving, the file path should be checked and the .GIS extension should be retained for the image.

The relative merit of a classification should be based on how well the classifier is able to re-assign the training pixels to their designated class (Fig. 19) and, most importantly, on the agreement between the classified image (.GIS) and the operator’s interpretation of the BE image. The .GIS image is read into MultiSpec as a “Multispectral” type image, and the class assignments are shown with distinct colors, as in Fig. 20. The color of any phase can be changed by double clicking it in the class list and setting its color with the color picker. If the segmentation is acceptable, this image can be saved as a TIFF file (*File*→*Save Image to TIFF*). **Note:** The file must be saved in TIFF format because that is the only format that retains the index values that are needed for the final analysis steps.

Step 7: Save the project. Select the *File*→*Save Project As* menu item to which will retain all the efforts and results of the segmentation process. Even if a segmentation attempt is deemed unsuccessful, the project can be reloaded later and modified to add training fields, delete fields, run alternate classification algorithms, or even exclude specific images to see if the classification can be improved.

3.4 Cleaning up the segmented image

Even after the image segmentation in MultiSpec, some incorrectly assigned pixels are commonly found. Especially along grain boundaries or particle edges, contrast artifacts in the original SEM BE image can cause pixels to be incorrectly classified. These effects are ideally minimized beforehand by careful adjustment of brightness and contrast settings during acquisition of the SEM BE image. In this example (Figs. 20 and 21), the edge effects created a problem for the Maximum Likelihood classifier based upon inspection of the segmented image. The Fisher Linear Likelihood classifier generated a more accurate grouping of pixels but still had some incorrectly assigned pixels along the edges and within the belite grains. If not too severe, incorrectly assigned pixels may be removed after segmentation by using some of the smoothing filters in ImageJ. Threshold Blur

TRAINING CLASS PERFORMANCE (Resubstitution Method)											
Project Class Name	Class Number	Reference Accuracy (%)	Number Samples	Number of Samples in Class							
				1 Alite	2 Belite	3 Aluminate	4 Ferrite	5 Periclase	6 Arcanite	7 Aphthitalite	8 Void
Alite	1	96.0	7561	7257	304	0	0	0	0	0	0
Belite	2	97.1	9596	278	9318	0	0	0	0	0	0
Aluminate	3	100.0	1005	0	0	1005	0	0	0	0	0
Ferrite	4	97.5	1561	15	0	24	1522	0	0	0	0
Periclase	5	99.9	1914	0	1	0	0	1913	0	0	0
Arcanite	6	99.5	221	0	0	0	0	0	220	1	0
Aphthitalite	7	99.5	205	0	0	0	0	0	1	204	0
Void	8	100.0	10918	0	0	0	0	0	0	0	10918
TOTAL			32981	7550	9623	1029	1522	1913	221	205	10918
Reliability Accuracy (%)*				96.1	96.8	97.7	100.0	100.0	99.5	99.5	100.0
OVERALL CLASS PERFORMANCE (32357 / 32981) = 98.1%											
Kappa Statistic (X100) = 97.5%. Kappa Variance = 0.000001.											
CLASS DISTRIBUTION FOR SELECTED AREA											
Class	Number Samples	Percent									
1 Alite	331,916	42.21									
2 Belite	278,062	35.36									
3 Aluminate	18,830	2.39									
4 Ferrite	78,845	10.03									
5 Periclase	26,449	3.36									
6 Arcanite	3,839	0.49									
7 Aphthitalite	1,361	0.17									
8 Void	47,130	5.99									

Figure 19: MultiSpec classification table, or accuracy matrix, shows the classification set assignment accuracy, incorrectly assigned pixel counts, an overall accuracy assessment by the Kappa statistic, and the area fraction for each class [12]. Data shown here are based on one image, so no uncertainty statement is possible. The “Reliability Accuracy” value for each phase refers to the percentage of training set pixels that are correctly reclassified by the segmentation as the phase to which they were originally assigned.

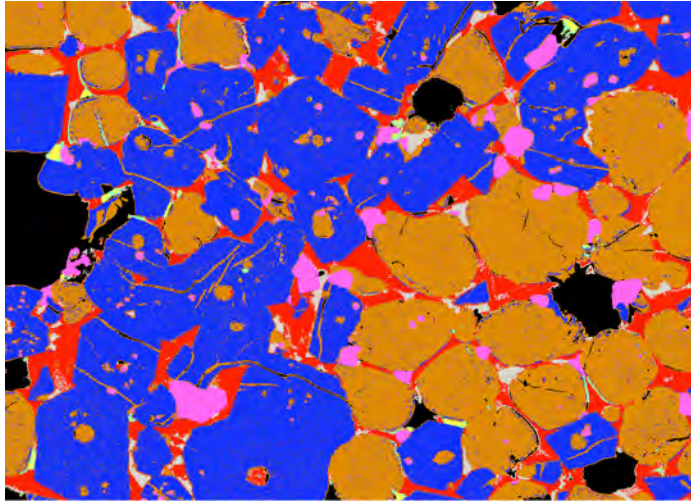


Figure 20: Comparing the segmented image to the original BE image (Fig. 4) indicates a successful segmentation. Some incorrectly assigned pixels occur at grain boundaries and within belite, which will be repaired in the final processing step. Field width is 256 μm .

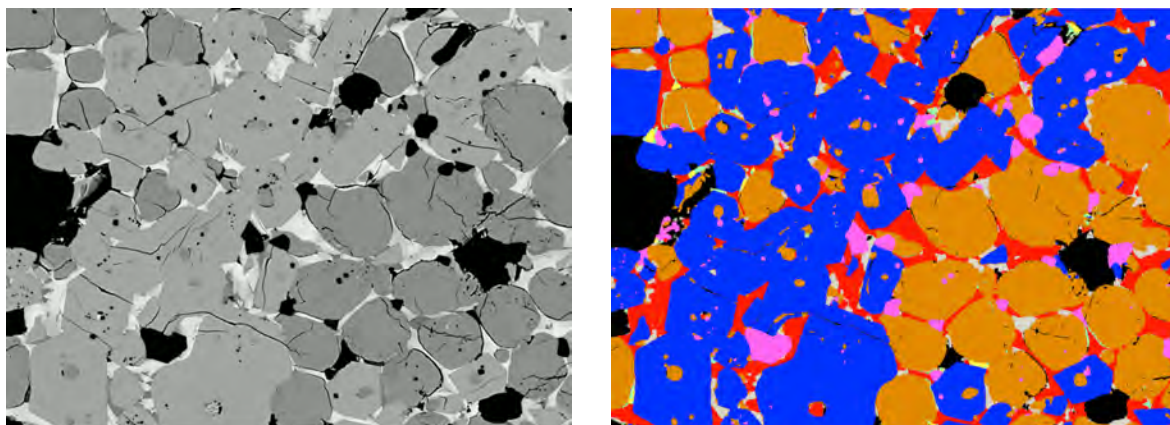


Figure 21: Original SEM BE image (left) and the processed, segmented indexed image (right) for comparison. Segmentation used the Fisher Linear Likelihood algorithm. Field width is 256 μm .

works well for minor edge effects by ignoring pixels that deviate from the mean and by allowing one to specify the kernel radius (start with 2 or 3), threshold (1, 2, or larger because this is an indexed image and the values differ by increments of 1), softness (affects the edge blur) and strength (number of times to apply the filter). After the edge effects have been reduced or eliminated in the .GIS file, save this and a TIFF and also write the ASCII Indexed file: *File*→*Save As*→*Text Image* that will be used in the image analysis. If needed, the .GIS file in Multispec or the *MS.TIF file in ImageJ can be recalled to see which index value corresponds to each phase.

The completed segmentation with edge effects removed and original BE image are presented in Fig. 21 to illustrate the final segmentation results. The image is color-coded and indexed with alite (blue, 1), belite (brown, 2), aluminates (white, 3), ferrite (red, 4), periclase (pink, 5), arcanite (blue-green, 6), aphtitalite (yellow, 7), and porosity (black, 8).

3.5 Quantitative Image Analysis

The final result of phase segmentation is a 2D color image that identifies each pixel with an integer index associated with its assigned phase. Quantitative analysis can be performed on such an image to calculate, for example

1. the area fraction of each phase (on a total solids basis)
2. the perimeter fraction of each phase (on a total solid boundary length basis)
3. the spatial distribution of each phase, quantified by correlation functions
4. the possible percolation, or connectivity, of each phase

Many, if not all, of these operations can be performed by built-in functions, such as generating a histogram and list from the indexed image or augmenting ImageJ with Java plugins such as the correlation function. However, most of these plugins have been developed and optimized for

image processing in other fields, especially biology, and are not well-documented or validated for use with clinker or cement microstructure images. As an alternative, NIST has developed a simple, fast computer program specifically for performing quantitative image analysis on clinker or cement microstructures. The program, called MicroChar, is available for Windows or Mac OS X computers, performs all these calculations with minimal intervention by the user. Use of MicroChar is described in the following section.

3.5.1 Installing MicroChar

MicroChar can be downloaded as disk image (on Mac OS X) or installer (on Windows).

Installation on Mac OS X. Double click the disk image to mount it. This will open a window as shown in Fig. 22. The application can be installed by dragging its icon to the Applications folder.

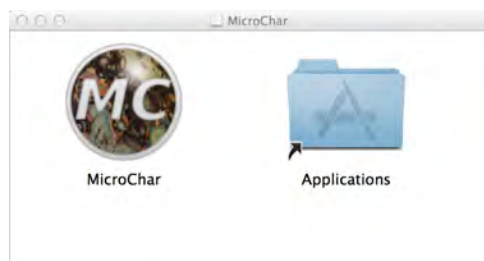


Figure 22: Installation of MicroChar on Mac OS X computers.

Installation on Windows. Double click the installer. If the user accepts the disclaimer, then choose a folder in which to install the application folder. After installation, a shortcut icon will be placed on the Desktop and in the Start Menu.

3.5.2 Using MicroChar

Launch MicroChar by double-clicking its icon. A window will open as shown in Fig. 23. Mousing over many of the items in the window will display a tooltip. For more context-specific information, click on the blue question mark icon in the toolbar and then click on the window item about which you want more information.

To begin a session, click on the blue folder icon in the upper left toolbar (or type Ctrl-O, to open the indexed image resulting from phase segmentation. The application works equally well on indexed images either of clinker or of powdered cement embedded in epoxy, but it analyzes the void space and perimeter identification differently for the two kinds of images. Therefore, after file selection, check the “Clinker image” checkbox only if the image is a clinker nodule; otherwise leave it unchecked. Specify the image resolution in terms of the width of a single pixel in micrometer (μm) units. The pixel dimension should be known at the time that the SEM image

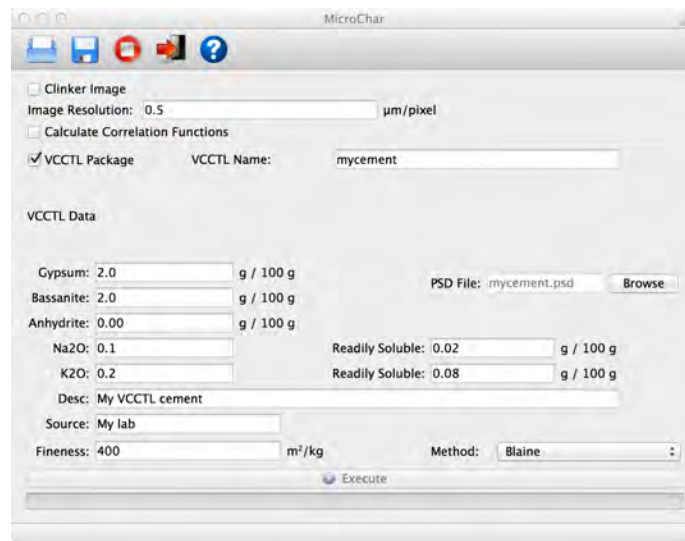


Figure 23: MicroChar main window.

is acquired, and is necessary to associate a length scale with the correlation functions that will be calculated if the corresponding checkbox is activated.

The remaining items in the window, which are grayed out by default, are related to data needed to create a cement data package for the Virtual Cement and Concrete Testing Laboratory. These items, which can be activated only for cement images by clicking the “VCCTL Package” checkbox, are beyond the scope of this document. Readers who are interested in using VCCTL software should consult the VCCTL software documentation [21].

Calculations begin by clicking the Execute button at the bottom of the window. The program reads the image file and records all the phase index numbers. When these have been collected, the user is prompted to associate each index with a known phase, as shown in Fig. 24. A default collection is offered, but each phase can be manually assigned by selecting the desired phase from the pulldown menu next to each phase id found in the image. Click the OK button when the desired selections have been made.

MicroChar proceeds automatically to perform the following sequence of operations:

1. The area of each phase is calculated and normalized by the total solid area to yield its area fraction on a total solids basis.
2. The mass fraction of each phase, on a total solids basis, is calculated from the area fractions and knowledge of the density of each phase.
3. The perimeter of each phase is calculated. For clinker images, the perimeter is defined as the boundary of the given phase with any other phase, including porosity; for cement images, the perimeter is defined as the boundary of the given phase only with interparticle porosity, because such boundaries determine the reactive surface area with water.
4. False color PNG images are created of (a) the microstructure and (b) the phase perimeters.



Figure 24: Phase identification is accomplished in MicroChar by accepting the default settings or by selecting the phases from the series of pull down menus.

- Two-point correlation functions, also known as autocorrelation functions in the field of signal processing, are calculated for each phase (only if the checkbox was activated).
- The program halts and prompts you to save your work if you wish, which you may do by clicking on the disk icon in the tool bar or by typing Ctrl-S.

As it proceeds through this sequence, MicroChar writes a collection of files to catalog the results of its calculations. These files, written to the same folder as the original indexed image, all have the same root name as the indexed image but different file extensions, as shown in Fig. 25.

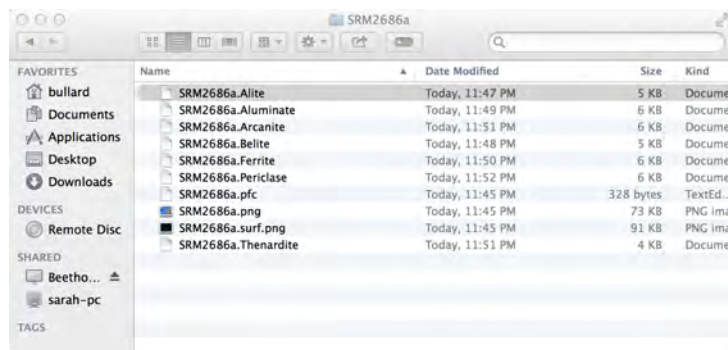


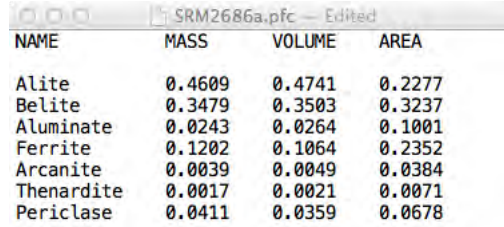
Figure 25: Files produced by MicroChar store the results of its calculations.

Three types of files are produced for clinker images:

- a file ending with 'pfc'⁵, which contain the mass, area, and perimeter fractions of each phase in the microstructure on a total solids basis, as shown in Fig. 25;
- files ending with 'png' or 'surf.png', which are the color images of the microstructure and perimeter, respectively, examples of which are shown in Fig. 26; and

⁵The extension 'pfc' is an acronym for phase fractions of cement (or clinker).

- files ending with a phase name, which store the two-point correlation function results for that phase (see example in Fig. 27).



NAME	MASS	VOLUME	AREA
Alite	0.4609	0.4741	0.2277
Belite	0.3479	0.3503	0.3237
Aluminate	0.0243	0.0264	0.1001
Ferrite	0.1202	0.1064	0.2352
Arcanite	0.0039	0.0049	0.0384
Thenardite	0.0017	0.0021	0.0071
Periclase	0.0411	0.0359	0.0678

Figure 26: Contents of the pfc file for the segmented image of SRM 2686a in Fig. 20. Here the column heading “Volume” corresponds to the phase area fractions and “Area” to the perimeter fraction.

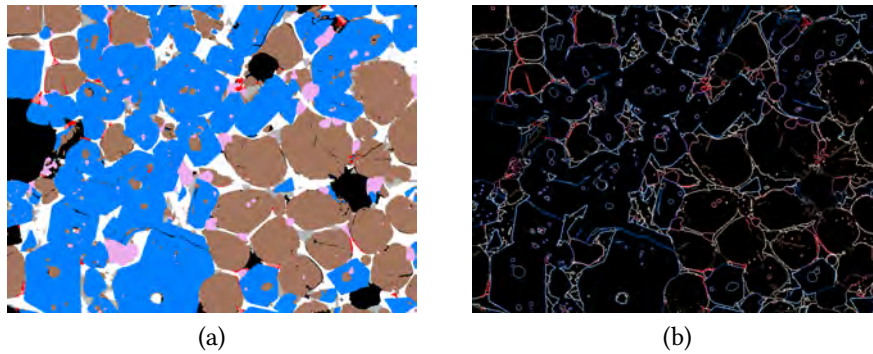


Figure 27: (a) False color PNG image of SRM 2686 microstructure, and (b) the phase boundaries. Field width is 256 μm .

3.5.3 Two-point correlation functions

The resulting data files from MicroChar are mostly self-explanatory, as shown in Figs. 26–28. However, correlation functions may be less familiar to the reader, so they will now be explained in more detail.

The two-point correlation function for a phase, $S_2(r)$, is the probability that two randomly selected points in the image, separated by a distance r , both lie within that phase. In random composite materials, S_2 has some generic features that can be used to characterize the spatial distribution of the phase. For example, when $r = 0$, the points coincide; the probability of a randomly selected point lying within a phase in a 2D image is equal to the area fraction, ϕ , of that phase, on a total area basis. Therefore, $S_2(0) = \phi$, that is, the y -intercept of the plot is equal

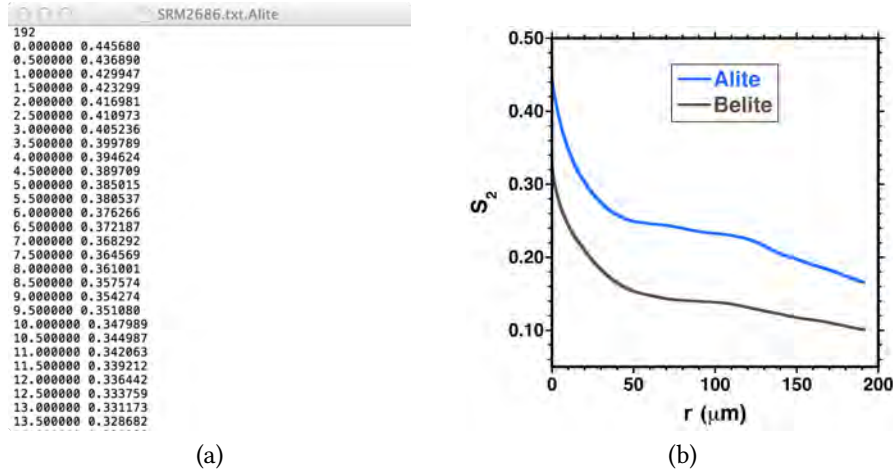


Figure 28: (a) Contents of the alite two-point correlation function data file for SRM 2686a image in Fig. 20 with distance in the first column and probability density in the second column; (b) plot of the two-point correlation function S_2 for alite and for belite in the SRM 2686a image (right).

to the phase's area fraction. A second property of $S_2(r)$, which will not be proven here, is that its limiting slope as $r \rightarrow 0$ is directly proportional to the phase's boundary length per unit area, Σ . In particular, for granular media the exact relation can be shown to be [3]

$$\lim_{r \rightarrow 0^+} \frac{dS_2}{dr} = -\frac{\Sigma}{4} \quad (1)$$

A third property of S_2 is that, at sufficiently large distances between the two points in a random microstructure, the phase identity of each point should be independent of the other. In other words, the phase distribution should be uncorrelated at large distances. When two events are statistically independent, the joint probability is equal to the product of the (unconditional) individual event probabilities. As stated earlier, the probability of a single point lying within a phase is the phase's area fraction, ϕ , so S_2 at sufficiently large distances should converge to ϕ^2 .

Examination of the plot in Fig. 27 shows that $S_2(0) = 0.4457$ for alite, which therefore is alite's area fraction on a total image area basis. Furthermore, the slope at $r = 0$ for alite is approximately $-0.0158 \mu\text{m}^{-1}$, which provides a semiquantitative indication of the specific boundary area of alite in the image. Finally, the plot indicates that S_2 for neither alite nor belite appears to be converging to ϕ^2 , which is 0.198 for alite and 0.1024 for belite. This can be interpreted to mean that the spatial distribution of each phase is still somewhat correlated at distances as large as $200 \mu\text{m}$. A cursory inspection of Fig. 21 suggests that both alite and belite are clustered over a fairly large length scale, so it is not surprising that the phase distributions are still correlated at $200 \mu\text{m}$. This hypothesis can be tested by examining a larger segmented image field of SRM 2686a, as discussed in Section 3.6.

Fig. 29 shows the two-point correlation functions for the minority phases arcanite and periclase. This plot highlights two other features of two-point correlation functions. First, the cor-

relation functions appear to be converging to values of about 10^{-3} for periclase and about 10^{-4} for arcanite at distances no greater than about $100\text{ }\mu\text{m}$. At $r = 0$, the values of ϕ for periclase and arcanite are 0.0337 and 0.0046, respectively. Squaring these values gives 0.0011 for periclase and 0.00002 for arcanite, both values of which are reasonably close to the long-distance values. Therefore, both periclase and arcanite are concluded to lose any spatial correlation at distances of about $100\text{ }\mu\text{m}$.

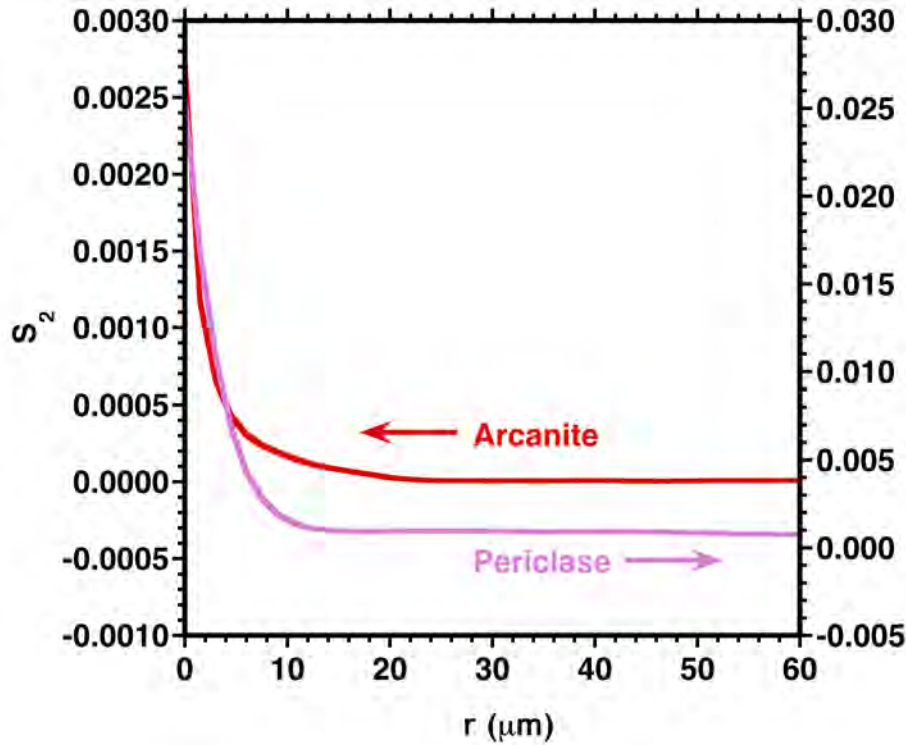


Figure 29: Two-point correlation functions for periclase and arcanite in SRM 2686a. Note the two different scales on the y -axes.

The second feature of the two-point correlation functions in Fig. 29 is the appearance of a local minimum at short distances followed by a small-amplitude oscillation in the curves. The periodic local minima are characteristic of granular media and of non-overlapping domains in composites, such as periclase and arcanite in SRM 2686a (Fig. 21). In such materials, the distance at which the first local minimum occurs corresponds to about half the average equivalent radius of the domain, and the distance at which the following local maximum happens corresponds to the average domain spacing in the microstructure [3]. Inspection of Fig. 29 suggests that the average equivalent radius of periclase and arcanite domains is about $31\text{ }\mu\text{m}$ and about $18\text{ }\mu\text{m}$, respectively. Likewise, the average domain spacings of periclase and arcanite are about $40\text{ }\mu\text{m}$ and about $27\text{ }\mu\text{m}$, respectively. Note that these same kinds of features cannot be extracted from correlation functions when the phases are significantly correlated over long distances, as appears to be the case for alite and belite in Figs. 27 and 28.

3.6 Larger Image Field

Image analysis statistics may improve by using larger fields of view that can capture more of the intrinsic heterogeneity within the microstructure. For example, Fig. 30 shows a larger image field for SRM 2686a, which was acquired at 200 \times magnification, with a resolution of 1.5 $\mu\text{m}/\text{pixel}$.

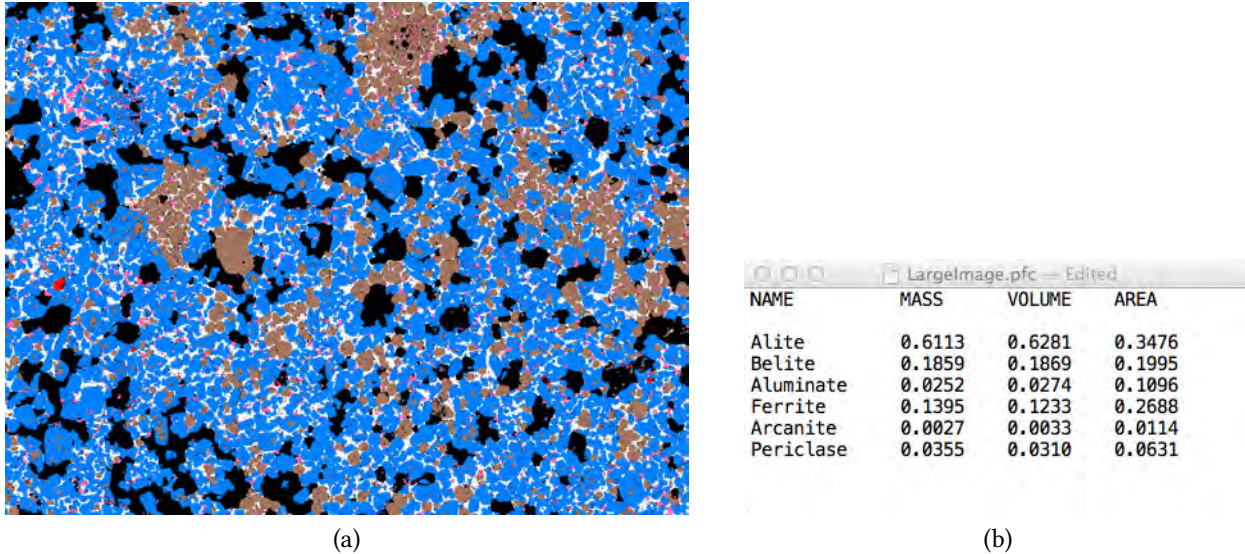


Figure 30: Larger image field of SRM 2686a. Magnification 300 \times , 1024 \times 768 pixels. (a) False color PNG image, and (b) the phase mass, volume, and area fractions. Field width is 1.536 mm.

Notice that the abundances of alite and belite, especially, (Fig. 30(b)) are significantly different than those measured on the smaller image in earlier sections (Fig. 20). For example, the volume fraction of alite is 32 % greater, and that of belite 47 % less, than in the smaller image. One would ordinarily place more confidence in phase fractions measured on larger fields of view, which should reduce errors due to heterogeneity in the microstructure. As already discussed, alite and belite in the SRM 2686a clinker microstructure are still significantly correlated over the field of view in the smaller image, as shown by the fact that their two-point correlation functions do not converge to the square of their volume fraction at longer distances (Fig. 28). Therefore, one should be skeptical that the volume fractions of these phases measured on the smaller image are representative of the material.

Fig. ?? shows the two-point correlation functions for alite and belite measured on the larger field of view in Fig. 30(a). In contrast to the corresponding functions for the smaller image, the correlation function for both alite and belite do converge, well within the field of view, to the square of their respective volume fractions. This result suggests that the larger image in Fig. 30(a) adequately captures all the heterogeneity within the material and, therefore, that phase abundance estimates based on this image are probably more representative of their true values. In fact, as shown in Table 3, the clinker phase mass fractions estimated from Fig. 30 are quite close to the

certified values⁶ for this material.

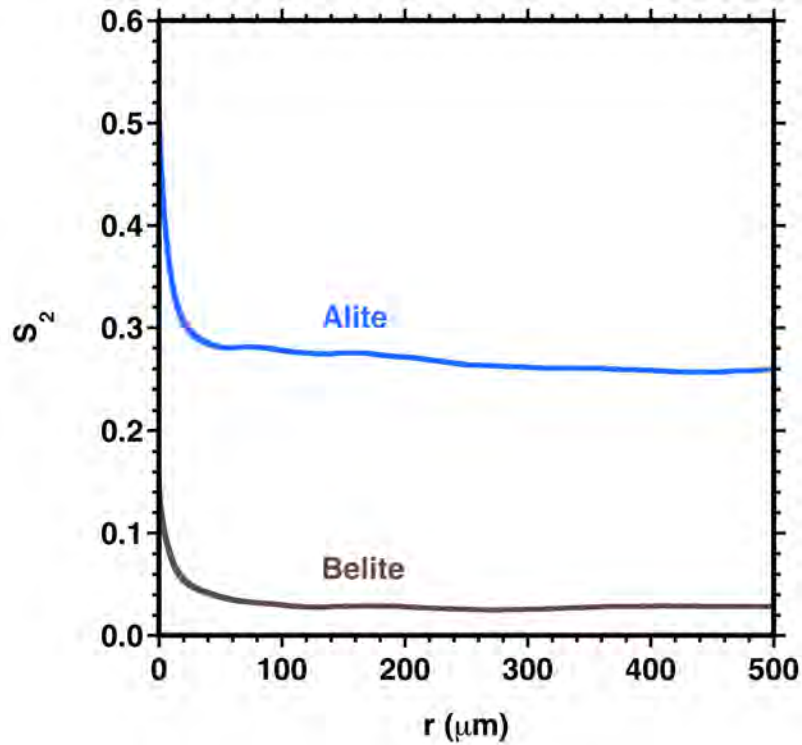


Figure 31: Two-point correlation functions calculated for alite and belite using the large image field of SRM 2686a shown in Fig. 30.

Table 3: Comparison of clinker phase mass fractions, expressed as a percentage of total solids, estimated for SRM 2686a from the larger field of view in Fig. 30 to the certified values [15]. Measurements are based on one image field, so no uncertainty estimate is given.

Phase	Measured (%)	Certified (%)	Difference (%)
Alite	61.13	63.35	-2.22
Belite	18.59	18.68	-0.09
Aluminate	2.52	2.46	0.06
Ferrite	13.95	10.76	3.19
Periclase	3.55	3.40	0.15
Arcanite	0.27	0.27	0.00

⁶Certified values of SRM characteristics, although obviously having some measurement uncertainty, are conventionally treated as “ground truth” for comparison purposes.

3.7 Multiple Image Statistics for SRM 2686a

When larger image fields like the one in Fig. 30 are unavailable or are difficult to capture due to resolution limits of the microscope, intrinsic heterogeneity can also be accommodated by analyzing multiple image fields at higher magnification. Running averages and standard deviations are tracked and checked for consistency with the SRM certificate and XRD values for the mass fraction of each clinker phase.⁷ The results, by imaging field, are presented graphically in Fig. 32; results for each image field are also presented in Table 4 along with the certified values and $2\text{-}\sigma$ uncertainties (95 % coverage). Consideration must be made that we are working with a medium-grained, heterogeneous material with this clinker and that heterogeneity will be expressed as a field-to-field variability in the measured results. Materials that are heterogeneous at coarser length scales will have larger field-to-field variability which, as already shown in the previous section, can be reduced by using larger imaging areas. However, image field enlargement cannot continue indefinitely without compromising the resolution and losing grain boundary definition. In fact, multi-phase microstructures will always have field-to-field variability that generally increases as the image area is reduced. Therefore, uncertainties measured on multiple image fields provide an estimate of the heterogeneity length scale relative to the image area: larger uncertainties correspond to greater heterogeneity at the chosen length scale.

Another means of visualizing the results is with the box plot (Fig. 33), where the median value is used for its resistance to outliers, and is identified by the “X”, the interquartile range (*i.e.*, “middle half”) of the data are represented by the body of the box, and the extremes (minimum and maximum) are represented by the ends of the straight lines projecting out of the box. The stars on the plot correspond to the certified values, also tabulated in Table 3. The constant sum effect is also apparent in Fig. 33 with the values varying inversely with the major phase estimates. This is one possible source of bias with normalized estimate methodologies. A cumulative mean estimate (running average) is presented in Table 4 and in graphical form in Fig. 32. For this clinker and sampling conditions, the values appear to stabilize after four fields of view and the final estimates are close in value to the certified values.

⁷Consistency with a certified value is taken to mean that the mean value of a measured characteristic lies within one standard deviation of the certified value.

Table 4: SRM 2686a phase fractions expressed as a mass percent by field and a running average.

Field	Mass Percent by Field					
	Alite	Belite	Aluminate	Ferrite	Periclase	Alkali sulfate
1	66.4	18.8	1.8	9.4	3.1	0.6
2	68.1	16.4	1.9	9.4	3.1	1.0
3	64.1	18.7	2.2	11.0	3.0	1.0
4	64.4	17.6	2.5	11.7	3.0	0.8
5	65.1	17.0	2.4	11.5	3.0	0.8
6	65.3	16.3	2.6	11.9	3.1	0.8
7	64.3	17.0	2.7	12.2	3.0	0.8
8	63.5	18.0	2.8	12.0	3.0	0.7
9	64.3	17.3	2.7	12.0	3.0	0.6
10	64.7	17.5	2.6	11.6	3.0	0.6
11	64.3	17.6	2.6	11.9	3.0	0.6
12	64.8	17.3	2.5	11.7	3.0	0.6
13	64.8	17.0	2.6	11.9	3.0	0.6
14	64.9	17.1	2.5	11.8	3.1	0.7
	Mass Percent: Running Average					
1	66.4	18.8	1.8	9.4	3.1	0.6
2	67.2	17.6	1.9	9.4	3.1	0.8
3	66.2	18.0	2.0	9.9	3.1	0.8
4	65.8	17.9	2.1	10.4	3.0	0.8
5	65.6	17.7	2.2	10.6	3.0	0.8
6	65.6	17.5	2.2	10.8	3.1	0.8
7	65.4	17.4	2.3	11.0	3.0	0.8
8	65.2	17.5	2.4	11.1	3.0	0.8
9	65.1	17.5	2.4	11.2	3.0	0.8
10	65.0	17.5	2.4	11.3	3.0	0.8
11	65.0	17.5	2.5	11.3	3.0	0.8
12	64.9	17.5	2.5	11.4	3.0	0.7
13	64.9	17.4	2.5	11.4	3.0	0.7
14	64.9	17.4	2.5	11.4	3.0	0.7
2- σ	2.2	1.4	0.6	1.8	0.2	0.2
<i>Certificate</i>	63.53	18.80	2.46	10.80	3.40	0.86
<i>2U_c</i>	1.04	1.10	0.39	0.84	0.23	0.17

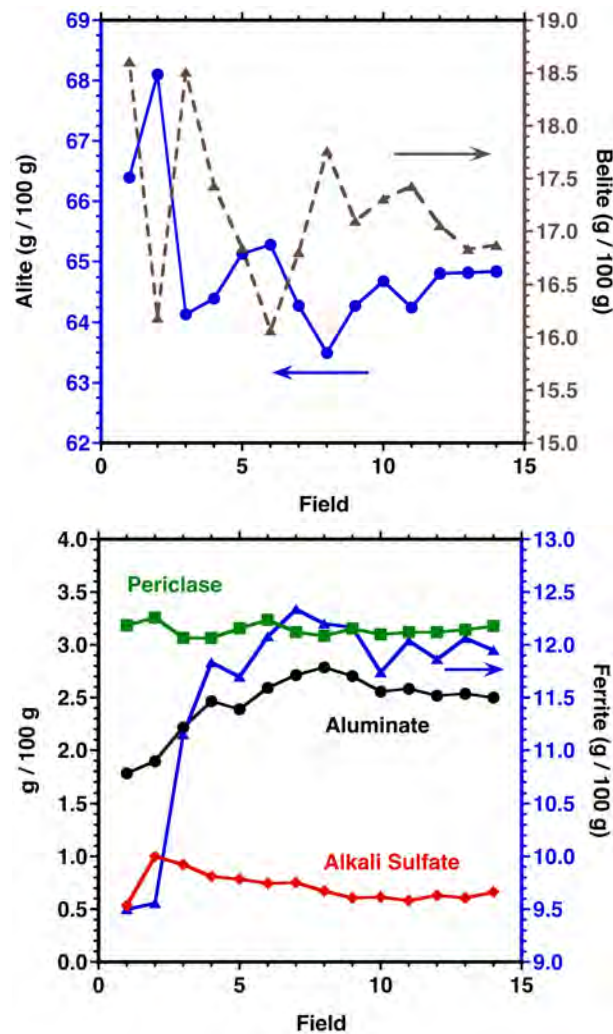


Figure 32: Running average plots for SEM/IA analysis of SRM2686a shows values beginning to stabilize after about five image fields.

Appendix A Step-by Step Summary for Clinker Analysis

ImageJ is used to preview the SEM BE and XR images and to interactively make some adjustments to the background and noise by improving the image quality. We always retain the original images and use the *File*→*Save As* command to save a modified image. Appending the filename with an M to indicate the operation performed on the image indicates that it has been modified. By appending the filename with an operation code, the images will appear together in the directory, allowing for easy viewing of the available images. Always save as a TIFF file format to eliminate any image quality loss with subsequent processing operations.

1. Read images individually or by drag-and-drop with ImageJ.

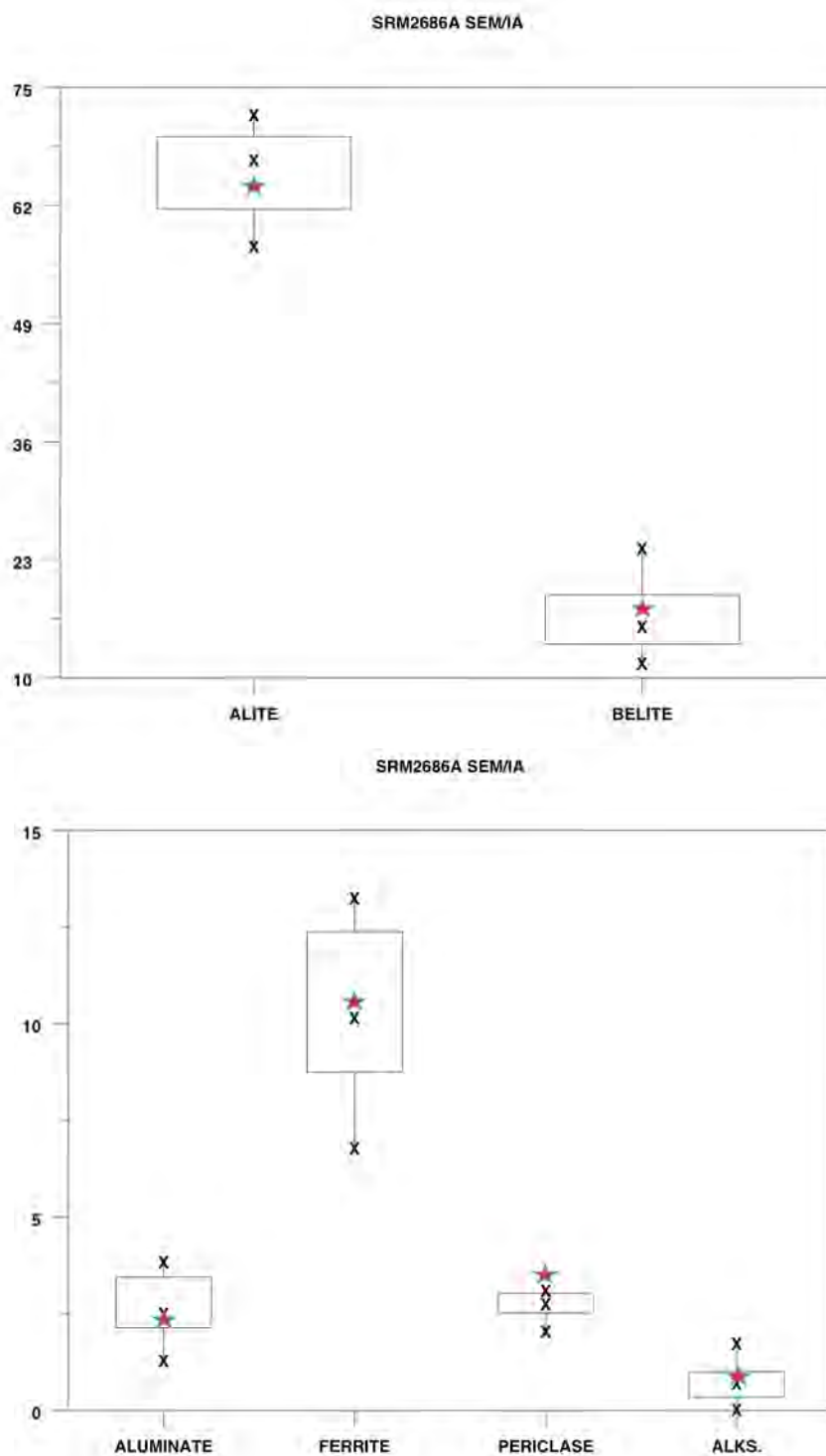


Figure 33: Box plots by phase for SEM analysis of SRM 2686a. Stars indicate certified values.

2. Tile images to arrange all on the monitor (*Window→Tile*)
3. Assign a gray LUT to each image (*Image→Lookup Table→Grays*)
4. Adjust each image's brightness and contrast to assess the noise associated with low element concentration or the background (image noise): *Image→Adjust→Brightness Contrast*
5. Subtract background noise with operation (*Process→Subtract*) using the preview check box in the Subtract operation window to interactively select the noise level. When acceptable, select *OK*.
6. Clean up any noise by filtering. The *Despeckle* and the *Remove Outliers* commands under *Process→Noise* to remove isolated pixels or small pixel groups. The median filter (*Process→Filters→Median*) or the *Thresholded Blur* will also work well to reduce image noise while retaining edge details. Apply any filtering lightly as edge blur may result in problems during the segmentation phase. Save the modified image using *File→Save As→TIFF*, appending the original file name with an "M" to indicate this file has been modified, so that the original is not over-written.
7. Use MultiSpec to generate a segmented, indexed image where each pixel is uniquely assigned to a class to which it most likely belongs based upon a user-developed training set of data. An abbreviated set of steps, which will be detailed below include (a) reading image files, (b) linking files, (c) designating phase classes, (c) establishing training fields for each class, (d) selecting a classification algorithm, (e) evaluating the classification, (f) saving the project, and (g) saving the classified image as an indexed, segmented TIFF file. This image file will then be used for the image analysis for determining phase area fraction, phase mass fraction, and phase perimeter fraction. The resulting image and phase-related data are useful characteristics of the microstructure and for introduction into simulation models like VCCTL [4, 21] or THAMES [5].
8. Read initial image as a multispectral type (*File→Open Image*), and check "multispectral type" box.

Under "Multispectral Display Specifications" accept the defaults with the exception of the "Enhancement" section, where you can opt to not change the image (the usual), clip it on the low and high end, or user selected clipping.

9. Link the set of X-ray images deemed useful in making a segmentation: *File→Open Image*. **Note:** This operation requires selecting "Link to active image window" from the drop-down box.

Select the X-ray images by clicking on them individually. Remember to select the modified ones (M). I use a standard image sequence so I can recall the exact image source in the virtual linked files (BEI, Al, Mg, K, Na, S) or write it down. They can be named later if necessary and excluded in the classification if desired. Click on the *Cancel* button to complete the linking.

10. Save the image set (*Processor*→*Reformat*→*Rectify Image*)

Use the window defaults (you could attempt to correct any displaced images here if needed), make sure the path is correct and provide a name, retaining the .LAN extension. Use the original file name to keep them together in a listing. If you do not include the extension, the file will be written without one and will not be recognized for future Read operations.

11. Open the .LAN image set for review, assigning classes and training fields, and classification (*File*→*Open Image*)

You will then see a window labeled “Multispectral Display Specifications,” where you can assign the channels to a color (R G B) and enhance the images by clipping or transformation. We did the enhancements using ImageJ since Multispec seems to apply a single set of operations to each image. View the image using different channel/color combinations. The most useful are:

- BE, Mg, Al — alite, belite, aluminate, ferrite, periclase, lime, voids
- BE, K, S — alkali sulfates, calcium sulfates

12. Establish training classes (*Processor*→*Statistics*)

Accept the defaults in the “Set Project Options” window by clicking *OK*.

In the new Project window you will see a Class Designation at the top. Enter the list of classes here by boxing in a region in the image for each, selecting “Add to List” and providing a name. The classes are listed based on this sequence and the ultimate index value used for VCCTL or THAMES, following this convention:

1 = alite	2 = belite	3 = aluminate	4 = ferrite
5 = periclase	6 = arcanite	7 = aphthitalite	8 = void

Record the index designations for later use as some phases will be absent from some materials.

Subclasses can be created—for example, alkali sulfate could contain sub-classes arcanite (potassium sulfate) and aphthitalite (potassium, sodium sulfate).

Add training classes then by selecting the class, boxing in more regions, and specifying “Add to List”. The more training pixels, the better the class characteristics are defined.

13. Classify (*Processor*→*Classify*)

Specify the “Minimum Euclidian Distance” algorithm as it works consistently well. Check the box “Write Classification Results” to Disk File and check the path, retaining the .GIS extension for this image.

Initial quality check is the percent re-assignment of the training set pixels and the quality of the class assignment seen in the .GIS image. The .GIS image is read into Multispec as a Multispectral type image and you will see the class assignments with distinct colors. The colors may be changed by double clicking on the class list followed by setting the color using the color picker.

14. Save the work as a Project

Even if not successful, you can go back and add training fields, delete fields, run alternate classification algorithms, and even exclude specific images to see if it can be improved.

15. Save the .GIS file as a TIFF file.

This preserves the color assignments for the phases and the index values. Do not save these in the .JPG format as the index values and colors will not be saved. You also do not want to overwrite any files so append the file name with a MS suffix.

16. Clean up any mis-assigned pixels using a surface blur filter that retains edge details.

The plugin “Thresholded Blur” works well for this by ignoring pixels that deviate from the mean and by allowing you to specify the kernel size (radius, start with 2 or 3), threshold (1 or 2 as this is an indexed image and the values differ by 1), softness (affects the edge blur) and strength (number of times to apply).

17. Read the TIFF file into ImageJ and write the ASCII Indexed file (*File→Save As→Text Image*).

You now have an ASCII file with the phase index values. If needed, you can recall the .GIS file in Multispec or the *MS.TIF file in ImageJ to see which index value corresponds to each phase.

References

- [1] “ASTM C 183: Standard Practice for Sampling and the Amount of Testing of Hydraulic Cement”. In: *Annual Book of ASTM Standards*. Vol. 4.01. West Conshohocken, PA: ASTM International, 2014.
- [2] P. H. Bates and A. A. Klein. *Properties of the Calcium Silicates and Calcium Aluminates Occurring in Normal Portland Cement*. Technological Papers of the Bureau of Standards 78. Washington, D.C.: U.S. Bureau of Standards, 1917.
- [3] J. G. Berryman and S. C. Blair. “Use of Digital Image Analysis to Estimate Fluid Permeability of Porous Materials: Application of Two-Point Correlation Functions”. In: *J. Appl. Phys.* 60.6 (1986), pp. 1930–1938.
- [4] J. W. Bullard and P. E. Stutzman. “Analysis of CCRL Portland Cement Proficiency Samples Number 151 and Number 152 Using the Virtual Cement and Concrete Testing Laboratory”. In: *Cem. Concr. Res.* 36 (2006), pp. 1548–1555.

-
- [5] J. W. Bullard et al. "Coupling Thermodynamics and Digital Image Models to Simulate Hydration and Microstructure Development of Portland Cement Pastes". In: *J. Mater. Res.* 26 (2011), pp. 609–622.
- [6] D. H. Campbell. *Microscopical Examination and Interpretation of Portland Cement and Clinker*. 2nd. Skokie, IL: Portland Cement Association, 1999.
- [7] M. A. Delesse. "Procédé Mécanique pour Déterminer la Composition des Roches (Mechanical Methods for Determining the Composition of Rocks)". In: *Annales des Mines* 13 (4th series) (1866), pp. 379–388.
- [8] J. I. Goldstein et al. *Scanning Electron Microscopy and X-Ray Microanalysis*. 2nd. New York: Plenum Press, 1981.
- [9] F. Hofmänner. *Microstructure of Portland Cement Clinker*. Holderbank, Switzerland: Holderbank Management and Consulting, Ltd., 1975.
- [10] *ImageJ: Image Processing and Analysis in Java*. Accessed: 2015-03-16. URL: <http://imagej.nih.gov/ij/>.
- [11] H. Insley and V. D. Fréchette. *Microscopy of Ceramics and Cements*. New York: Academic Press, 1955.
- [12] D. A. Landgrebe. *Signal Theory Methods in Multispectral Remote Sensing*. New York: Wiley Interscience, 2003.
- [13] Henri Le Châtelier. *Experimental Researches on the Constitution of Hydraulic Mortars (English Translation)*. New York: McGraw-Hill, 1905.
- [14] *MultiSpec: A Freeware Multispectral Image Data Analysis System*. Accessed: 2015-03-16. URL: <https://engineering.purdue.edu/~biehl/MultiSpec/>.
- [15] *NIST Standard Reference Material 2686a—Portland Cement Clinker*. Accessed: 2015-04-21. URL: https://www-s.nist.gov/srmors/view_detail.cfm?srm=2686a.
- [16] P. E. Stutzman. "Microscopy of Clinker and Hydraulic Cements". In: *Rev. Mineralogy Geochem.* 74.1 (2012), pp. 101–146.
- [17] P. E. Stutzman. "Scanning Electron Microscopy Imaging of Hydraulic Cement Microstructure". In: *Cem. Concr. Composites* 26.8 (2004), pp. 957–966.
- [18] P. E. Stutzman and J. R. Clifton. "Specimen Preparation for Scanning Electron Microscopy". In: *Proceedings of the 21st International Conference on Cement Microscopy*. Ed. by L. Jany and A. Nisperos. Las Vega, NV: International Cement Microscopy Association, Apr. 1999, pp. 10–22.
- [19] P. E. Stutzman, G. Lespinasse, and S. Leigh. *Compositional Analysis and Certification of NIST Reference Material Clinker 2686a*. Technical Note. Washington, D.C.: National Institute of Standards and Technology, 2008.
- [20] *Thresholded Blur: Another Edge-Preserving Averaging (Smoothing) Algorithm, also Known as Surface Blur*. Accessed: 2015-03-16. URL: <http://imagejdocu.tudor.lu/doku.php?id=plugin:filter:thresholded%5C.blur:start%5C&do=export%5C.pdf>.

REFERENCES

- [21] *VCCTL Software*. Accessed: 2015-03-16. URL: <http://www.nist.gov/el/building-materials/evcctl.cfm>.